POLITECNICO DI TORINO

MASTER's Degree
in Aerospace Engineering

MASTER's Degree Thesis

Influence factors on CubeSat lifetime deployed from ISS

Supervisors
prof. Lorenzo Casalino

Candidate
Jacopo Cerzosimo

Academic Year 2022-2023

Summary

The first five CubeSats were released from the Kibō module of the International Space Station (ISS) via the JAXA J-SSOD deployer on 4^{th} October 2012. A CubeSat, as a U-factor standard size, has been revolutionizing access to low-Earth orbit (LEO). Since then, a recurrent need of knowing about the lifetime of CubeSat in orbit. Thus, the main objective of this thesis is to explore the main parameter influencing the lifetime of CubeSat deployed from the ISS. The work is performed in collaboration with Nanoracks Space Outpost Europe, which offers the opportunity to deploy satellites from the ISS. Therefore, the spacecraft parameters together with the effect of the deployment and perturbation due to the Space environment are the main elements of this study. An estimation is performed via the Systems Tool Kit (STK) software of AGI and choosing Astrogator as the orbit propagator which allows simulating the release of the CubeSats, including the ΔV provided by the deployer and the possibility of varying satellite parameters during the decay. The subjects of the analysis are single-unit, double-unit and triple-unit CubeSat also known as 1U, 2U and 3U which are the most deployed in recent years. Considering tumbling satellites, deployed in 2022, an orbital decay of 277, 337 and 357 days is estimated for 1U, 2U and 3U respectively. Then, a longer lifetime by switching the satellite to the minimum drag mode, resulting in an increase of 100 days for 1U and 600 days for 3U could be reached. In conclusion, predicting the satellite's attitude may help in the estimation. Nevertheless, the prediction of solar activity is still another element to be taken into account for an improvement of the accuracy and precision of the simulation.

Acknowledgements

I wish to thank Nanoracks Space Outpost Europe for giving me the opportunity to carry out this work. I would also like to thank AGI and Fabrizio Gemma for allowing me to exploit the STK functionality for the analysis of this study through a student licence. I thank Giuseppe Corrao for his valuable advice on the functionality of STK and the orbital decay topic. Finally, yet importantly, I thank my family and friends for always being by my side.

To all sea wolves who, after a shipwreck, resume their voyage

Table of Contents

Acronyms

AFSPC Air Force Space Command

AGI Ansys Government Initiatives

DRAMA Debris Risk Assessment and Mitigation Analysis

DRAO Dominion Radio Astrophysical Observatory

EGM2008 Earth Gravitational Model 2008

EUV Extreme Ultraviolet Radiation

HPOP High Precision Orbit Propagator

ISS International Space Station

JAXA Japanese Aerospace and in Exploration Agency

JEM Japanese Experiment Module

JEMRMS JEM Remote Manipulator System

J-SSOD JEM Small Satellite Orbital Deployer

LEO Low Earth Orbit

MCS Mission Control Sequence

MPEP Multi-Purpose Experiment Platform

NOAA National Oceanic and Atmospheric Administration

NRCSD Nanoracks CubeSat Deployer

NRSOE Nanoracks Space Outpost Europe

RAAN Right Ascension of the Ascending Node

RKF Runge Kutta Fehlberg

RKF 7(8) Runge Kutta Fehlberg integration method of 7th order with 8th order error control for the integration step size

SFU Solar Flux Unit

SRP Solar Radiation Pressure

STK Systems Tool Kit

TLE Two-Line Elements

USSTRATCOM U.S. Strategic Command

UTCG Gregorian Coordinate Universal Time

Symbols

a Semi-major axis

$\bar{\boldsymbol{a}}_{\boldsymbol{p}}$ Vector of the total acceleration caused by other forces acting on the satellite

$\boldsymbol{A}_p$ Planetary amplitude

Az Azimuth

$\boldsymbol{A}_{\odot}$ Exposed area to Sun of satellite

b Semi-minor axis

$\bar{\boldsymbol{B}}$ Vector constant of integration in the trajectory equation

$\boldsymbol{B}^*$ Adjusted value of ballistic coefficient using the reference value of the atmospheric density

c Speed of light

$\boldsymbol{C_D}$ Drag coefficient

$\boldsymbol{c_r}$ Coefficient of reflectivity

e Eccentricity

E Energy

El Elevation

$\boldsymbol{E_m}$ Specific mechanical energy

F Primary focus if elliptic conic section

$\bar{\boldsymbol{F}}_G$ Gravitational force on m due to M in the two-body problem

$\boldsymbol{F_{10.7}}$ Solar flux index

G Universal gravitational constant

$\bar{\boldsymbol{h}}$ Vector of specific angular momentum

i Inclination

$\boldsymbol{J_n}$ Coefficient in Vinti equation to be determined by experimental observation

$\boldsymbol{K_p}$ Planetary index

$\boldsymbol{L_a}$ Geocentric latitude

m Mass of satellite

M Mass of central body

n Mean motion

N Number of orbits completed by a satellite in one day

p Semi-latus rectum

$\boldsymbol{P_n}$ Legendre polynomials

$\boldsymbol{R_\oplus}$ Earth radius

$\ddot{\bar{\boldsymbol{r}}}$ Vector acceleration of the mass measured with respect to an inertial reference frame

$\bar{\boldsymbol{r}}$ Vector from M and m in the two-body problem

r Module of the Vector from M and m in the two-body problem

$\boldsymbol{r_a}$ Radius of apogee

$\boldsymbol{r_p}$ Radius of perigee

SF Solar radiation constant

$\boldsymbol{Xa}$ Cross-sectional area or drag area

$\boldsymbol{\beta}$ Ballistic coefficient

$\boldsymbol{\mu}$ Gravitaional parameter

$\boldsymbol{\nu}$ True anomaly

$\boldsymbol{\Pi}$ Orbit period

$\boldsymbol{\rho}$ Air density

$\boldsymbol{\phi}$ Vinti potential function

$\boldsymbol{\omega}$ Argument of periapsis

$\boldsymbol{\Omega}$ Longitudine or right ascension of the ascending node (RAAN)

Chapter 1

Introduction

The work developed for the purpose of this thesis is carried out in collaboration with Nanoracks Space Outpost Europe (NRSOE), a Space company which provides three different options to deploy satellites from the International Space Station (ISS) according to their size: Nanoracks CubeSat Deployer (NRCSD) for CubeSats, Nanoracks Kaber MicroSat Deployer (Kaber) for MicroSatellites and Nanoracks Bishop Airlock for larger SmallSats. In particular, this work focuses on the orbital decay of the CubeSats, which growth is enlarging. Therefore, this chapter introduces the definition of CubeSats, the analysis of methods and mechanisms for releasing satellites into Space, and the explanation of the objectives of this work.

1.1 CubeSat Definition

A CubeSat is a satellite with a standardized shape called a unit, U. The size of a unit is $10\,cm \times 10\,cm \times 10\,cm$ with a typical weight of less than $1.33\,kg$ [1]. The concept of CubeSats originated from a collaboration between California Polytechnic State University in San Luis Obispo and Stanford University in Stanford, California. For the first time, a small educational platform called "CubeSat" was developed. Over the years, it has played a key role in the "democratization" of Space, making Space exploration and research accessible for universities and scientists [1]. This development is based on the low cost of manufacturing and putting CubeSats into orbit. Although CubeSats originally consisted of a single cube called a 1U, other different combinations as shown in figure 1.1, have been developed due to their widespread use in recent years [2].

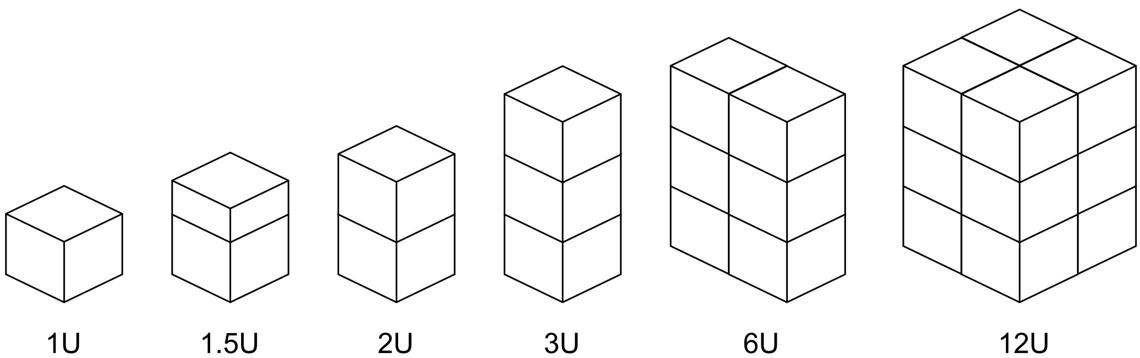

Figure 1.1: CubeSat unit possible combinations. Credit NASA [2]

The advantage of these larger CubeSats lies in the possibility of obtaining more science at a lower cost, due to the additional volume, power and overall increase in capacity. Today, after their physical expansion, CubeSats belong to the common category of small satellites (a satellite with a mass of less than 180 kg according to the Small Spacecraft Technology Programme) according to the mass definition of the sub-category: a CubeSat with a mass greater than 10 kg is a microsatellite, otherwise, a nanosatellite [2].

1.2 Deploying satellites from ISS

With the spread of the CubeSat concept, a large market for adapters and dispensers to compactly accommodate CubeSats on existing launchers was created [2]. The purpose of these technologies is both to mechanically interface the CubeSat to the launcher and to deploy it. The method to bring a satellite in Space integrated into the launch vehicle or separation system is called *rideshare*. In general, the choice of this way of releasing CubeSats into orbit implies total dependence on the customer of the primary spacecraft, who can decide whether to share the journey and how and when to deploy the secondary payload. In addition, the secondary payload must comply with the requirement not to damage the first payload or other satellites in the case of multi-mission launches. This may include restrictions on the design of the CubeSat.

By designing a small satellite launcher installed on the ISS and then demonstrating the ability to deploy a satellite from it successfully, the Japan Aerospace and Exploration Agency (JAXA) revolutionized the way small satellites are ejected in LEO. Specifically, as shown in figure 1.2, the Japanese Experiment Module (JEM) Small Satellite Orbital Deployer (J-SSOD) uses the JEM Remote Manipulator System (JEMRMS), which is a robotic arm, to position itself away from the station and safely deploy satellites [1].

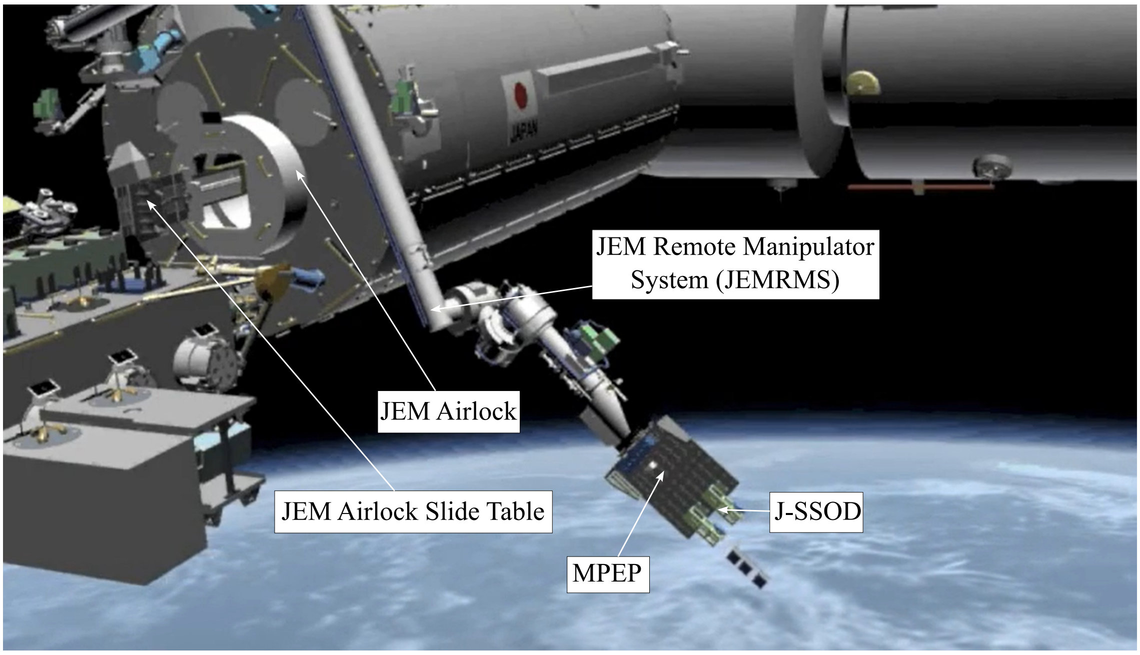

Figure 1.2: Deployment of 1U using JEMRMS and J-SSOD platform. Credit JAXA

Unlike *rideshare*, deploying from ISS implies:

- *The independence of the launch* enables the best time to eject the small satellite to be chosen without affecting the timing of the leading satellite. It is possible to exploit the regularly scheduled cargo resupply flights on which CubeSats can easily travel.
- *A moderate vibration environment* enables satellites not to have to pass stringent vibration tests. Satellites are delivered to the ISS in soft bags (Cargo Transfer Bags) buffered with packing materials. As a consequence, the level of vibrations they are subjected to is lower than when they are deployed from the launch vehicle.
- *The final satellite checkout* ensures its safety before deployment. Before use, astronauts can perform quality checks on the hardware.

In particular, the second and third features allow designers to choose electrical parts without traditional Space classifications, thus saving money and accelerating new space-qualified technology. This mainly refers to small satellite developers, because some of them, such as university students, for instance, cannot afford to use expensive aerospace-rated electrical parts to pass vibration tests.

The adoption of satellite deployment from the ISS has increased the use of Space Station deployments by potential developers of small satellites. As a result, universities, companies and other non-traditional space users are finding economic access to space [1]. In fact, since 2018, in addition to J-SSOD, other platforms have been used, such as Nanoracks CubeSat Deployer, developed by Nanoracks LLC, and CYCLOPS, developed by NASA [1]. As for the NRCSD, it is a self-contained CubeSat deployment system designed to accommodate any combination of CubeSats up to a maximum volume of 6U, or a single 6U CubeSat in the 1×6×1U configuration [3]. Specifically, as shown in figure 1.3 it is a rectangular "silo" that consists of four sidewalls, a base plate, a pusher plate assembly with an ejection spring, two access panels, two doors, and a primary release mechanism [3]. There is also an NRCSD DoubleWide which can accommodate CubeSats up to 12U (2×6U).

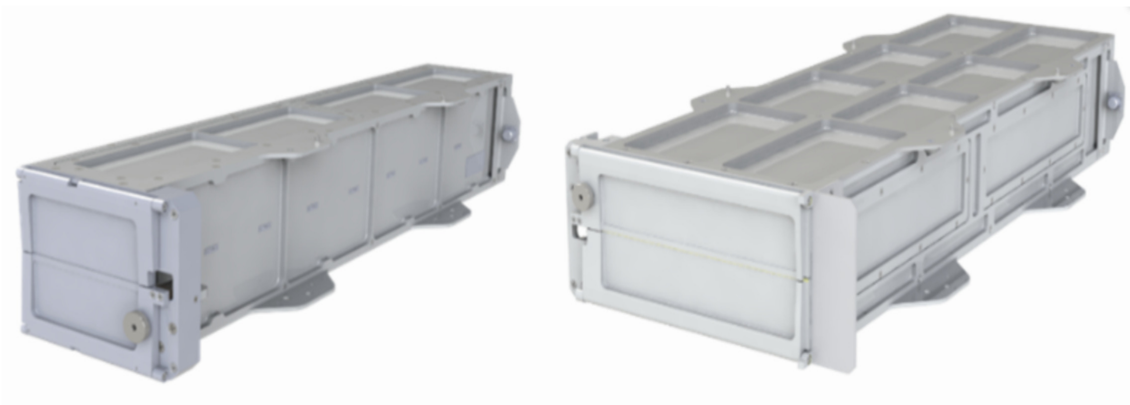

Figure 1.3: NRCSD and DoubleWide version. Credit [3]

Payload integration takes place on the ground, where the CubeSats are mechanically and electrically isolated from the supply vehicles, the ISS and the ISS crew. As far as deployment is concerned, the deployer is moved outside the airlock of the Kibō module on a sliding table. Specifically, the NRCSD mounts on the Multi-Purpose

Experiment Platform (MPEP), which in turn mounts on the JEM Airlock Slide Table, which is grasped by the JEMRMS which moves it to the correct launch position, generally below the ISS and in the opposite direction to the ISS velocity vector to avoid potential contact with the ISS [3].

1.3 Objectives of the study

In contrast to the advantages of deploying CubeSats from the ISS, as seen in 1.2, the deployment altitude imposed by the ISS, between 400-420 km, generally implies a short lifetime for the satellites. At this altitude, perturbative forces, mainly atmospheric drag, reduce the energy of the satellite, which consequently moves to a smaller orbit. If satellites are not equipped with a propulsion system, they cannot avoid the inevitable re-entry into the atmosphere, i.e. the end of their life. A reliable prevision on the satellite's lifetime, i.e. the time that has elapsed since deployment to when it burns in the atmosphere is fundamental for customers who want to bring their experiment into Space. Since accurately predicting the decay of a satellite is very complex, mainly due to the high level of uncertainty in predicting atmospheric drag, this is one of the points of discussion during negotiations between NRSOE and customers. Therefore, it is fundamental to investigate the dynamic behind the orbital decay of satellites deployed from the ISS. Within the company, this study was treated in two different ways: a code development and a parametric study. The first involves the development of a code to estimate the lifetime of the satellites by implementing a general perturbation technique then integrated numerically with Runge Kutta 4, and is reported in [4]. The second method is reported in this thesis and concerns the lifetime analysis of CubeSat 1U, 2U and 3U without a propulsion system through a parametric analysis that took into account environmental perturbations and the physical properties of the satellite. To achieve this, several simulations were performed using the AGI Systems Tool Kit (STK) software, choosing Astrogator as the orbit propagator.

1.4 Lifetime estimation approach

According to the standardized methods to assess orbital lifetime [5] shown in figure 1.4, it's necessary to select the analysis method among high-precision numerical integration, rapid semi-analytical orbit propagation and numerical table look-up. While the latter is a simple look-up of tables, graphs and equations generated using the other 2 methods, the second exploits the definition of average orbital elements, semi-analytical orbit theory and an average ballistic coefficient model to ensure rapid integration with reasonable accuracy. Unlike semi-analytical propagation and table look-up, numerical propagation is high-fidelity but requires more calculation time. As previously mentioned, the former is chosen for this work and the analyses were performed with STK's Astrogator propagator. The numerical integration uses a numerical integrator and accounts for a detailed gravity model, third-body effects, solar radiation pressure and a detailed model of the satellite's ballistic coefficient. As will be seen in chapter 4, however, an average ballistic coefficient is adopted in this work due to the difficulty of obtaining its precise values. In addition to the ballistic characteristics of the spacecraft and the attitude rules, the initial orbital conditions and the atmosphere model are selected as input for the analysis method.

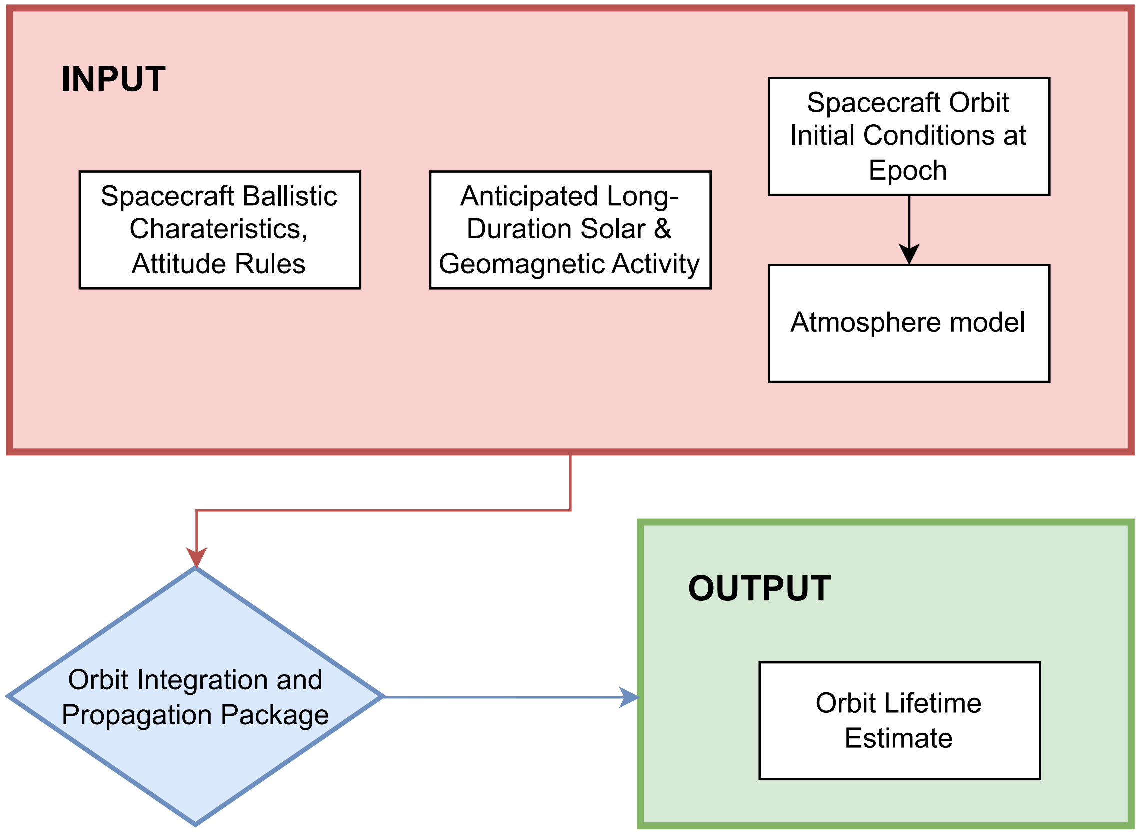

Figure 1.4: Lifetime estimation process

In particular, the choice of the appropriate atmosphere model to be incorporated into the orbit acceleration formulation is followed by the selection of the appropriate inputs to that model [5]. Therefore, it is important to choose an atmosphere model that accommodates solar activity variation to obtain more accurate results.

To execute the analysis, the process shown in Figure 1.4 is followed, while to study the effect of the parameters affecting the orbital decay, [6] and [7] are the main references.

Chapter 2

Orbital Dynamics

2.1 Two-Body Problem

A model for describing the motion of planets and later satellites is provided by Kepler's law, while Newton's law of universal gravitation is an explanation of such motion [8]. By applying the equation derived from the latter law and Newton's second law of motion, the equation of motion for planets and satellites is developed.

Newton's second law of motion states that "the time-rate change of momentum is proportional to the force impressed and is the same direction as that force" and for systems of constant mass is expressed mathematically by the equation 2.1:

$$\sum \bar{F} = m\ddot{\bar{r}} \tag{2.1}$$

where $\sum \bar{F}$ is the vector sum of all the forces acting on the mass and $\ddot{\bar{r}}$ is the vector acceleration of the mass measured with respect to an inertial reference frame.

Regarding the law of gravity, it states that "any two bodies attract one another with a force proportional to the product of their masses and inversely proportional to the square of the distance between them" and is expressed mathematically by the equation 2.2:

$$\bar{F}_g = -\frac{GMm}{r^2}\frac{\bar{r}}{r} \tag{2.2}$$

where $\bar{F}_g$ is the force on mass m due to mass M, $\bar{r}$ is the vector from M to m and G is the univeral gravitational constant roughly equal to $6.673 \times 10^{-20} \frac{km^3}{kg \cdot s^2}$.

It is assumed that the bodies are spherically symmetric and the gravitational forces are the only ones acting on the system and along the line joining the centre of two bodies. Specifically, the system, as shown in figure 2.1, consists of two bodies of masses M and m, known as the two-body problem. In addition, there are two coordinate systems, one inertial (**X'**,**Y'**,**Z'**) and the other (**X**,**Y**,**Z**) non-rotating, with axes parallel to the first and originating in the body of mass M. Applying Newton's law in the inertial reference frame and measuring the relative position, velocity and acceleration in (**X**,**Y**,**Z**), the equation of motion 2.3 is obtained:

$$\ddot{\bar{r}} + \frac{\mu}{r^3}\bar{r} = 0 \tag{2.3}$$

where μ is the gravitational parameter, i.e the product between M and G, and resulting from the assumption of $M >> m$. In fact, the mass of a satellite in Earth's

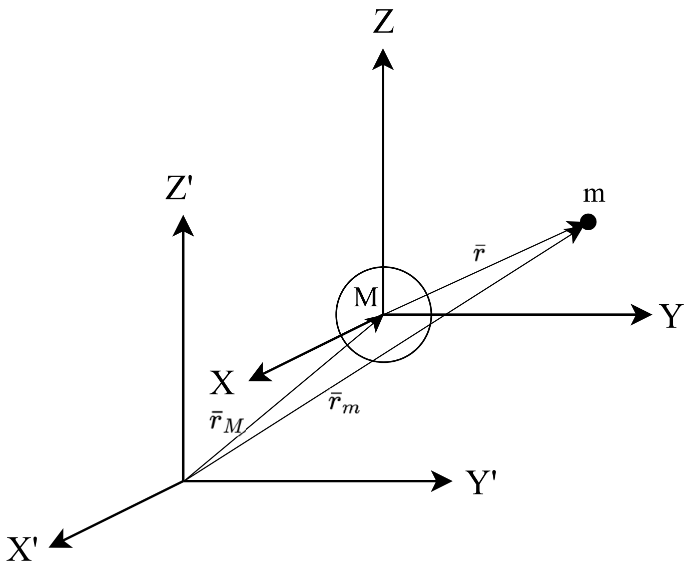

Figure 2.1: Relative motion of two-body problem

orbit is negligible compared to the mass of the Earth.
The equation 2.3 is a second-order non-linear vector differential equation describing a model in which a small mass (e.g. a satellite) moves in a gravitational field whose force is always directed towards the centre of a large mass (e.g. the Earth). Since one of the above assumptions implies the presence of only the gravitational force in the two-body system, and since a gravitational field is "conservative", the specific mechanical energy E of the satellite is conserved. In addition, the satellite's specific angular momentum $\bar{h}$ concerning the centre of the reference frame (**X**,**Y**,**Z**) is constant due to the radial direction of the gravitational force (i.e. there are no tangential forces that can change the angular momentum). Furthermore, from the definition of h, the satellite's motion must be confined to a plane that is fixed in space, the orbital plane.

2.1.1 The Trajectory Equation

It is possible to obtain easily a partial solution of the equation 2.3 by crossing this equation into $\bar{h}$ and performing several algebraic steps. The resulting equation 2.4 provides information on the size and shape of the orbit:

$$r = \frac{\frac{h^2}{\mu}}{1 + \left(\frac{B}{\mu}\right)\cos\nu} \tag{2.4}$$

where B is the module of the constant vector of integration $\bar{B}$ and ν is the angle between $\bar{B}$ and $\bar{r}$. The equation 2.4 is the trajectory equation expressed in polar coordinates where ν is the polar angle [8]. There is a similarity between equation 2.4 and the general equation of a conic section written in polar coordinates:

$$r = \frac{p}{1 + e\cos\nu} \tag{2.5}$$

where p is a geometric constant of the conic called semi-latus rectum, while e, which determines the type of conic, is called eccentricity. Therefore, not only is Kepler's first law ("the orbit of each planet is an ellipse, with the Sun at a focus") verified but the law is extendable to orbital motion along any conic section path.

A conic section may be defined as the curve of the intersection of a plane and a right circular cone [8]. Figure 2.2 shows a geometric representation of an elliptic conic section.

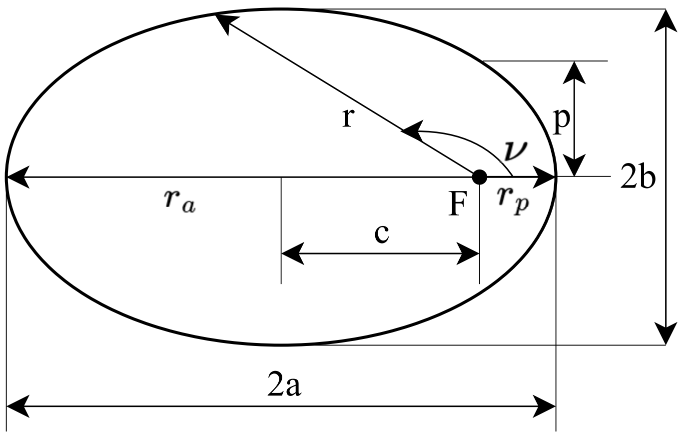

Figure 2.2: Elliptic conic section

The ellipse has two foci, where F is the primary focus (e.g. the Earth's centre for satellites' orbit) and F' is the secondary focus. Half the distance between foci is the dimension c, while a is the semi-major axis and b is the semi-minor axis of the ellipse. The distance from the primary focus to the farthest point of the ellipse is called the radius of apogee, r_a, and to the closest point of the ellipse is called the radius of perigee, r_p.

An ellipse is a closed curve, so an object along this orbit always travels the same path. The time it takes the satellite to complete one revolution around its orbit is called the period Π. It is expressed by the equation 2.6:

$$\Pi = 2\pi\sqrt{\frac{a^3}{\mu}} \tag{2.6}$$

In the case of a circular orbit, Π is expressed by the equation 2.7:

$$\Pi = 2\pi\sqrt{\frac{r^3}{\mu}} \tag{2.7}$$

The circular orbit is a special case of the ellipse in which the semi-major axis is constant and coincides with the radius.

Useful for analysis is also the definition of mean motion with units of radians per unit of time [9]. This is therefore the average angular velocity of change of the satellite in orbit. It is expressed by the equation 2.9:

$$n = \sqrt{\frac{\mu}{a^3}} \tag{2.8}$$

2.2 Satellite State

Defining the state of a satellite in space requires six components. Their collection is called either *state vector* or *element sets*. The former is usually associated with position and velocity vectors, while the latter is typically used with scalar magnitude and angular representations of the orbit and is called orbital elements [9]. Both refer to a particular coordinate frame. As far as *element sets* are concerned, the classical orbital elements, often called Keplerian elements, are the most common. Other element sets have been developed for convenience or to avoid the difficulties the classical orbital elements suffer for certain orbital geometries, such as two-line and equinoctial ones [9].

2.2.1 Classical Orbital Elements

Considering the orbit of an Earth satellite in the geocentric-equatorial system using **IJK** unit vectors, the classical set of six elements, shown in figure 2.3, is defined by [8]:

a, *semi-major axis* a is a constant defining the size of the conic orbit.

e, *eccentricity* e is a constant defining the shape of the conic orbit.

i, *inclination* i is the angle between the **K** unit vector and the angular moment vector $\bar{h}$.

Ω, *longitude or right ascension of the ascending node* Ω (RAAN) is the angle, in the fundamental plane, between the **I** unit vector and the point where the satellite crosses through the fundamental plane in a northerly direction (ascending node) measured counterclockwise when viewed from the north side of the fundamental plane.

ω, *argument of perigee* ω is the angle, in the plane of the satellite's orbit, between the ascending node and the periapsis point, measured in the direction of the satellite's motion.

ν, *true anomaly at epoch* ν is the angle, in the plane of the satellite's orbit, between perigee and the position of the satellite at a particular time called the epoch.

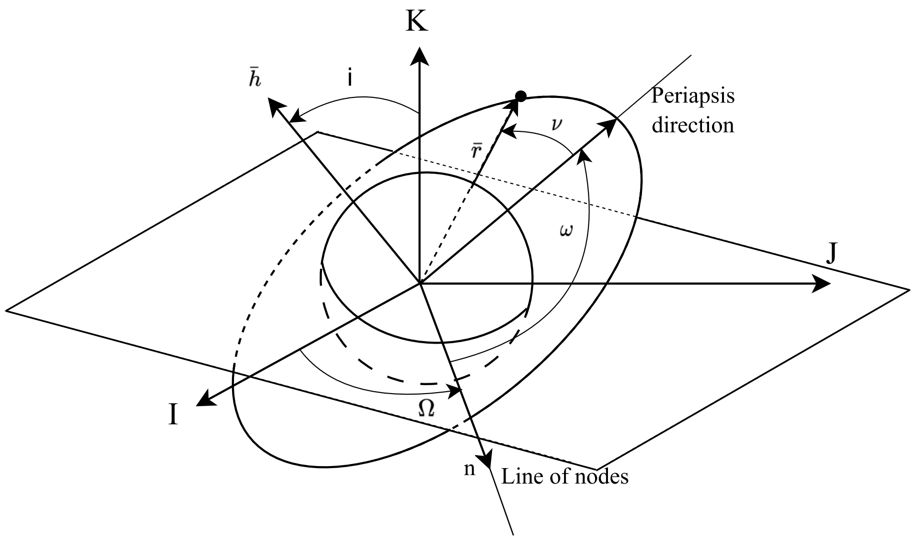

Figure 2.3: Keplerian orbital parameters

The first five elements are sufficient to completely describe the size, shape and orientation of an orbit, whereas the last is necessary to identify the position of the satellite along the orbit at a given time. Sometimes the semi-latus rectum p replaces a or time at perigee passage T, i.e. the time when the satellite was at perigee, replaces ν. Furthermore, the listed definitions are suitable also considering another coordinate system, only the definitions of unit vectors and the fundamental plane would be different.

2.2.2 Two-Line Element Sets

Two-line element sets (TLE) are available to the general public through Air Force Space Command (AFSPC) [9]. TLE sets describe the Space object's orbit at a specific epoch using a specific definition of the orbital parameters and are generated using the SGP4 perturbation model. TLE elements are collected in a table with 72 columns and two rows. The time unit is in Universal Time Coordinate (UTC), while the coordinate system should be considered a true-equator, mean equinox system In addition, the units of each variable in the table are different and specific to each measure.

Table 2.1: TLE sets line 1

Column	Description
01	Line number of element data
03-07	Satellite number
08	Classification (U=unclassified)
10, 11	International Designator (Last two digits of launch year)
12-14	International Designator (Launch number of the year)
15-17	International Designator (Piece of the launch)
19, 20	Epoch Year (Last two digits of year)
21-32	Epoch (Day of the year and fractional portion of the day)
34-43	First-time derivative of the mean motion
45-52	Second-time derivative of mean motion (decimal point assumed)
54-61	BSTAR drag term (decimal point assumed)
63	Ephemeris type
65-68	Element number
69	Checksum (letters, blanks, periods, plus signs=0; minus signs=1)

Specifically, from the definition of mean motion, which is different from that of subsection 2.1.1, it is possible to derive the period of the orbit:

$$\Pi = \frac{86400 \ s}{N} \tag{2.9}$$

where N is the number of orbits per day and the numerator represents the number of seconds in a day. Moreover, in table 2.1, BSTAR is an adjusted value of the ballistic coefficient using the reference value of the atmospheric density ρ_0 :

$$B^* = \frac{B\rho_0}{2} \tag{2.10}$$

Table 2.2: TLE sets line 2

Column	Description
01	Line number of element data
03-07	Satellite number
09-16	Orbital inclination (degrees)
18-25	Right ascension of the ascending node (degrees)
27-33	Orbital eccentricity (decimal point assumed)
35-42	Argument of perigee (degrees)
44-51	Mean anomaly (degrees)
53-63	Mean motion (orbit per day)
64-68	Revolution number at epoch (orbits)
69	Checksum (Modulo 10)

2.3 Perturbations

The theory of the two-body problem cannot resolve accurately the real-world trajectory problems [8]. Perturbations caused by other bodies and additional forces not considered result in the theoretical orbit being changed. In particular, perturbations are deviations from a normal, idealized, or undisturbed motion [9]. Fortunately, most orbital flight perturbations are predictable and analytically treatable. However, others require a stochastic approach, such as solar activity. Therefore, perturbation methods are essential to obtain more realistic results. There are two main categories of perturbation techniques, *special* and *general perturbations*. The former deal with the direct numerical integration of the equations of motion including all necessary perturbing accelerations, while the latter involve an analytical integration of series expansions of the perturbing acceleration [8]. Note that in the case of numerical integration, any perturbative acceleration can be considered. Considering *special perturbations*, the output refers to a specific problem or set of initial conditions, whereas in the case of *general perturbation*, the result provides more detail and covers many cases. This is particularly true when the calculations are of long duration.

2.3.1 Special Perturbation Techniques

Cowell's method is the simplest and most widespread *special perturbation technique* [8]. It consists of implementing the equations of motion of the studied object, including all perturbations, and then integrating them numerically step by step. Taking the perturbations into account in the two-body problem is possible by adding the perturbing accelerations as shown in the equation 2.11:

$$\ddot{\bar{r}} + \frac{\mu}{r^3}\bar{r} = \bar{a}_p \tag{2.11}$$

where $\bar{a}_p$ is the total acceleration caused by other forces acting on the satellite. Fortunately, the form of the equation 2.11 allows each effect to sum linearly. The equation 2.11 is known as the *Cowell's formulation* and is a second-order differential equation of motion that is numerically integrated, while the *Cowell's method* is a technique that uses the calculus of finite differences to perform the integration [9]. For numerical integration, the *Cowell's formulation* would be reduced to first-order differential equations 2.12:

$$\begin{aligned} \dot{\bar{r}} &= \bar{v} \\ \dot{\bar{v}} &= a_p - \frac{\mu}{r^3}\bar{r} \end{aligned} \tag{2.12}$$

where $\bar{r}$ and $\bar{v}$ are the radius and the velocity of a satellite with respect to the larger central body [8]. In addition, to solve the equations 2.12, it is necessary to use the vector components.

The main advantage of this method is its simplicity in formulation and implementation. However, solving the equation of motion in the vicinity of a large attractive body requires smaller integration steps, which affect the time and cumulative error. Furthermore, the velocity is rough $1/10^{th}$ that of Encke's method and is not suitable for lunar trajectories [8].

Encke's method isn't very popular today but it is historically relevant [9]. Instead of integrating the sum of all the acceleration, it integrates just the difference between the two-body acceleration and the perturbed acceleration. The perturbations to the orbit are integrated with cartesian elements. This method implies a reference orbit along which the object would move in the absence of all perturbating acceleration called the osculating orbit. The process continues until a rectification point where the osculating orbit is re-initialized. Integrating only between the osculating (two-body) orbit and the actual perturbed implies the magnitudes are much smaller and the computational precision is greater [9]. Therefore, the *Encke's method* is much faster than *Cowell's* due to taking larger integration step sizes when near a large attracting body [8]. Moreover, it is especially useful for interplanetary trajectories.

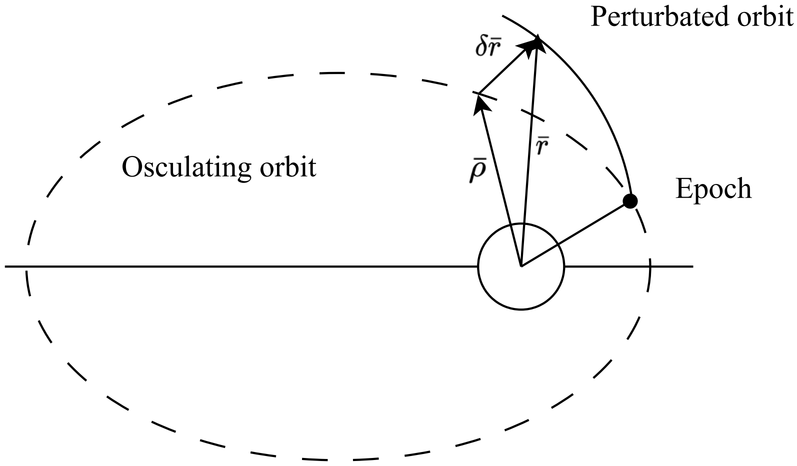

Figure 2.4: Encke's method

Considering the equation 2.11 as that for the true orbit and the equation 2.13 for the osculating orbit:

$$\ddot{\bar{\rho}} + \frac{\mu}{\rho^3}\bar{\rho} = 0 \tag{2.13}$$

the difference between the two accelerations is given by the equation 2.14:

$$\delta\dot{\bar{r}} = \bar{a}_p + \frac{\mu}{\rho^3}\left[\left(1 - \frac{\rho^3}{r^3}\right)\bar{r} - \delta\bar{r}\right] \tag{2.14}$$

Another interesting method involves the variation of parameters or elements and was first developed by Euler in 1748 [8]. It is recommended in the presence of small perturbing forces. While the previous methods refer to coordinates, this one concerns orbital elements or any set of parameters describing the state of the satellite. The latter is based on research into how the selected parameters vary over time due to perturbations. Therefore, analytical expressions of these variations are defined and then integrated numerically. Note that orbital parameters vary slowly concerning position and velocity over an entire orbit, so a larger integration step can be chosen in which total acceleration (as in Cowell's method) or perturbative acceleration (as in Encke's method) is integrated. Furthermore, a difference between this method and Encke's method is that in the latter the orbit is constant until rectification, whereas in the method of *parameter variation* the reference orbit changes continuously [8].

2.3.2 Numerical Integration Method

Before evaluating different numerical integration methods, it is important to know the type of errors involved. Rounding and truncation errors are the main types of errors. The former arises from the finite number of digits of any number that a computer can carry forward, while the latter are due to an inexact solution of the differential equation [8]. Note that a numerical integration is an exact solution of the difference equation, which imperfectly represents the true differential equation. In particular, the truncation error results from not using all the series expressions used in the integration method. This error is directly proportional to the value of the step size. Eventually, the rounding errors depend on the machine, whereas the truncation errors on the integration method.

Runge-Kutta, *Adams-Moulton*, *Gauss-Jackson* and *Adams-Bashforth* are some representative numerical integration methods. The former is a single-step method, while the others are multi-step. These latter require a single-step method to be started at the beginning and after each change in step size [8].

The most well-known numerical integrators are the *Runge-Kutta methods* originally presented by Carl Runge in 1895, and Wilhelm Kutta in 1901 [8]. They derive from a Taylor series, but differ from it in that, instead of having to derive application-specific formulae for the terms of the upper derivatives, they simply use the slope at different points within the range over which it is integrated. Equations 2.15 and 2.16 shows the classical fourth-order *Runge-Kutta method*:

$$x_{n+1} = x_n + \frac{1}{6}\left(k_1 + 2k_2 + 2k_3 + k_4\right) \tag{2.15}$$

where

$$\begin{aligned}
k_1 &= hf\left(t_n, x_n\right) \\
k_2 &= hf\left(t_n + \frac{h}{2}, x_n + \frac{k_1}{2}\right) \\
k_3 &= hf\left(t_n + \frac{h}{2}, x_n + \frac{k_2}{2}\right) \\
k_4 &= hf\left(t_n + h, x_n + k_3\right)
\end{aligned} \tag{2.16}$$

and n is the increment number.

Conventionally, a method is termed fourth-order if it's locally accurate to fourth-order, globally correct to third-order, has fifth-order local error and fourth-order global error [9]. Other forms are derived from the basic method, such as the *Runge-Kutta-Fehlberg* (RKF) method, which uses a variable step size. The main feature is to adjust h to keep local truncation errors within certain tolerances. At each step, the equations of motion are numerically integrated twice in a different order and the results are compared. If they are not reasonably close, the step size is modified to maintain a uniform difference in the evaluations along the orbit. The final result uses the initial values with a seventh order with eighth-order *Runge-Kutta*. This approach is optimal when studying highly eccentric orbits such as Molniya's. Without this variable step size, much time is lost in the vicinity of the apoapsis, when the integrator is taking too small a step. Likewise, the integrator may not use a sufficiently small step size at periapsis, where the satellite is travelling very fast [9].

In general, the *Runge-Kutta methods* are stable, easy to implement, have a relatively small truncation error, do not require a start-up procedure and the step size is easily changed. On the other hand, it is not easy to determine the truncation error and thus the correct step size.

Adams-Bashforth is a multistep "predictor-corrector" method. It uses a calculated predictor value $\bar{x}_n + 1$ to estimate a correct one [8]. The first value is substituted into the differential equation to obtain $\dot{\bar{x}}_n + 1$, which is used to calculate the correct value $\bar{x}_n + 1$. In general, multistep methods are faster than single-step methods, but they are more complex. The *Adams-Moulton method* adopts the *Adams-Bashforth* scheme by adding a fourth-order formula. The difference lies in using the correcting formula to find the correct value of $\bar{x}_n + 1$. In addition, it is possible to iterate over the correcting formula until there is no significant change in the value $\bar{x}_n + 1$. This method requires a single-step method to start with and the *Runge-Kutta* is the one suggested [8].

As far as the *Gauss-Jackson* method is concerned, it was developed for the integration of systems of second-order equations. Its predictor alone is generally more accurate than other methods, although it also includes a corrector. It also handles the effect of rounding errors well. However, it is more complex than other methods. It is one of the best for trajectory problems of the type *Cowell* and *Encke*. Instead, for integration of first-order equations such as occur in the *variation parameters method*, *Adams-Bashforth* or *Adams-Moulton* are more suitable.

2.3.3 Disturbing Forces

Several aspects shall be taken into account in the general equation of motion. The satellite may orbit in the Earth's atmosphere and therefore drag effects may be present. If the a of the satellite's orbit is large, solar radiation may be considered. The effects of the planet's non-spherical shape, third body and tides may be other sources of perturbations. To integrate Cowell's formulation numerically, mathematical models are required for each perturbing force. Therefore, this subsection derives analytical formulations of the accelerations resulting from the most common perturbative forces. Note that only the simplest forms are considered, and more complex and more accurate could be added.

The Non-spherical Earth

From the section 2.1, the Earth's gravitational potential is μ/r and is due to a spherically symmetrical body of mass, resulting in conical orbits. Actually, the

Earth is swollen at the equator, flattened at the poles and generally asymmetrical. According to Vinti [10], a potential function that takes into account the Earth's non-sphericity is expressed by the equation 2.17:

$$\phi = \frac{\mu}{r}\left[1 - \sum_{n=2}^{\infty} J_n \left(\frac{R_\oplus}{r}\right)^n P_n \sin La\right] \tag{2.17}$$

where μ is the gravitational parameter, J_n is the coefficients to be determined by experimental observation, $R_\oplus$ is the equator radius of Earth, P_n is the Legendre polynomials, La is the geocentric latitude and $\sin La$ is equal to z/r. Considering a geocentric, equatorial coordinate system, acceleration can be found from the potential using the equation 2.18:

$$\bar{a} = \nabla\phi = \frac{\delta\phi}{\delta x}\bar{I} + \frac{\delta\phi}{\delta y}\bar{J} + \frac{\delta\phi}{\delta z}\bar{K} \tag{2.18}$$

Note that by developing the partial derivative, one always obtains a first term which is the acceleration of the two-body problem and the remaining terms represent the perturbation accelerations resulting from the non-sphericity of the Earth. Regarding J_n, a representative set of values for the first seven is given by the equation 2.19 defined by the Earth Gravitational Model EGM2008 [11] (an ASCII file containing the Central Body geopotential model coefficients):

$$\begin{aligned} J_2 &= (1082.63) \times 10^{-6} \\ J_3 &= (-2.532) \times 10^{-6} \\ J_4 &= (-1.62) \times 10^{-6} \\ J_5 &= (-0.15 \pm 0.1) \times 10^{-6} \\ J_6 &= (0.57 \pm 0.1) \times 10^{-6} \\ J_7 &= (-0.44 \pm 0.1) \times 10^{-6} \end{aligned} \tag{2.19}$$

As observed, the confidence factor decreases beyond J_4. In particular, J_2 takes into account the fact that the Earth is flattened at the poles and J_3 that the southern hemisphere is more massive than the northern. Furthermore, J_2 causes regression of the node line and precession of the apsidal line of the satellite's orbit.

The equations 2.17 only include zonal harmonics, i.e. those harmonics that depend only on the mass distribution, which is symmetrical concerning the Earth's north-south axis (with no longitudinal dependence). There are other types of harmonics, tesseral harmonics that depend on both latitude and longitude and sectoral harmonics that depend only on longitude. The EGM2008-WGS84 version takes into account all three classes of harmonics.

Atmospheric Drag

Atmospheric drag mainly affects the motion of satellites in low Earth orbit (LEO). The effect of aerodynamic drag slowly reduces the energy of the orbit, which becomes smaller. The decrease in altitude implies an increase in drag. This triggers a chain effect that leads to an altitude so low that the satellite re-enters the atmosphere. Below about 120 km, the satellite's lifetime is very short and re-entry occurs rapidly. Instead, above 600 km the lifetime could be more than 10 years [12].

As shown in equation 2.20, the acceleration due to atmospheric drag force is opposite the direction of the satellite's velocity vector relative to the atmosphere:

$$\ddot{\bar{r}} = -\frac{1}{2}\frac{C_D XA}{m}\rho v_a^2 \frac{\dot{\bar{r}}_a}{v_a} \tag{2.20}$$

where C_D is a dimensionless quantity which reflects the satellite's susceptibility to drag forces, approximately equal to 2.2, called the drag coefficient [9]; ρ is the atmospheric density at each satellite altitude; XA is the exposed cross-sectional area, i.e. the area which is normal to the satellite's velocity vector; m is the satellite's mass; $\dot{\bar{r}}_a$ is the velocity vector relative to the rotating atmosphere, while v_a is its module. Specifically, $\dot{\bar{r}}_a$ is expressed by the equation 2.21 [9]:

$$\dot{\bar{r}}_a = \dot{\bar{r}} - \bar{\omega}_{\oplus} \times \bar{r} = [\dot{x} + \omega_{\oplus} y \quad \dot{y} - \omega_{\oplus} x \quad \dot{z}]^T \tag{2.21}$$

where $\dot{\bar{r}}$ is the inertial velocity, $\bar{\omega}_{\oplus}$ is the vector rate of rotation of the Earth and $\mathbf{x}$ and $\mathbf{y}$ refer to the geocentric, equatorial coordinate system This formulation may be complicated by the introduction of expressions for theoretical density, altitude above an oblate Earth, wind variation etc.

In the equation 2.20 appears the inverse of $\frac{m}{C_D A}$, usually called the ballistic coefficient β. It is another value that indicates the behaviour of satellites under drag effects. Its definition implies that the lower β is, the greater the drag effect on the motion of the satellite, and vice versa.

Drag is one of the significant sources of the unpredictability of the satellite's position and lifetime. This difficulty involves the variation of drag due to the attitude of the spacecraft and the dramatic influence of solar activity on the atmospheric density trend as altitude changes. Specifically, the density of the upper atmosphere is strongly affected by the interaction between the nature of the atmosphere's molecular structure, the incident solar flux, and geomagnetic interactions [9]. Solar flux is represented by Extreme Ultraviolet Radiation (EUV) arriving from the Sun, which heats the upper atmosphere. Instead, geomagnetic activity retardedly heats atmospheric particles created by collisions with energetically charged particles from the Sun. The heating of the atmosphere causes it to expand and rise so that the portion of the atmosphere at 200 km moves to, say, 250 km, representing a much denser atmosphere for a satellite at that altitude [12].

The level of solar flux and geomagnetic activity is difficult to predict, but very important for precise models. As just said, the contribution of solar flux to atmospheric density is mainly from EUV incoming from Sun. From 1940, scientists measure both EUV and incoming solar radiation with a wavelength of 10.7 cm, $F_{10.7}$ (f = 2800 MHz), originating in the same layers of the Sun's chromosphere and corona [9]. EUVs can't reach the Earth's surface because the atmosphere doesn't allow their transmission. On the other hand, Earth's atmosphere is transparent to $F_{10.7}$ radiation. The relative strength of F_{EUV}, from Earth-based measurements, is expressed in Solar Flux Units, SFU where:

$$1\,SFU = 1 \times 10^{-22}\frac{W}{m^2 Hz} \tag{2.22}$$

The most commonly accepted measurement of $F_{10.7}$ is distributed daily by the National Oceanic and Atmospheric Administration (NOAA) at the National Geophysical Data Center in Boulder, Colorado. Measurements were routinely made at the Algonquin Radio Observatory in Ottawa, Ontario, Canada from 1947 until 31^{th} May 1991 at 1700 UT. Since then, the measurements have been made at the Dominion Radio Astrophysical Observatory (DRAO) Penticton, British Columbia, Canada, at 2000 UT. Daily values are averaged to produce 81-day average values (3 solar rotations) denoted with a bar [9]. The solar flux data may be either observed (at the true Sun-Earth distance) or adjusted to 1.0 AU. The conversion is explicated by the equation 2.23:

$$F_{10.7}(obs) = \frac{F_{10.7}(adj)AU^2}{R_{\oplus}^2 - Sun} \tag{2.23}$$

Figure 2.5 shows the historical record of solar activity from 1957 to 3^{th} March 2022, obtained plotting the data of the *SpaceWeather.txt* file of STK.

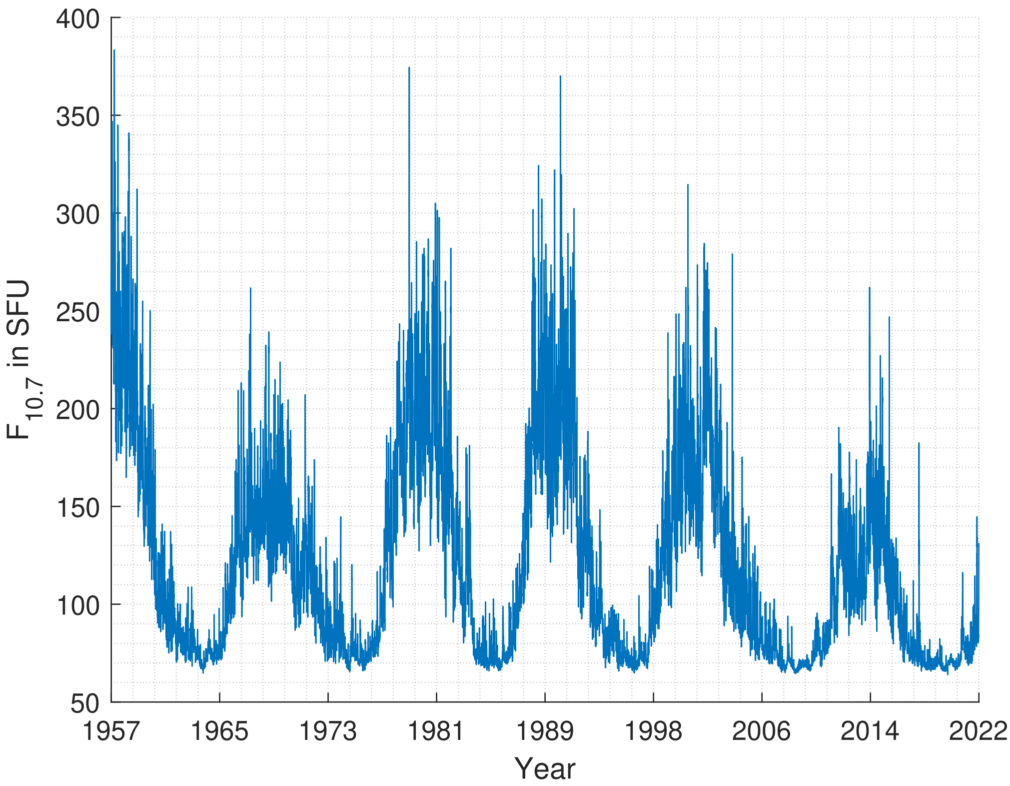

Figure 2.5: $F_{10.7}$ daily observed values over the years

As observed, typical values range from less than 70 to more than 300 SFU. Moreover, there are peaks that correspond approximately to solar maxima, i.e when the solar activity is intense and consequently the atmospheric density is high. There are also idle zones where an opposite trend occurs and consequently, the atmospheric density is low. Note that there is an 11-year solar cycle corresponding to the sunspot cycle, in which fluctuations in the number and size of sunspots and solar prominences are repeated due to the solar magnetic field completely reversing every 11 years [12]. This behaviour causes the amount of incoming solar radiation reaching the Earth to vary. Specifically, the level of $F_{10.7}$ is different from cycle to cycle and there are large month-to-month variations. Therefore, predicting the value at any specific future time is uncertain.

As far as geomagnetic activity is concerned, charged particles of any magnetic disturbance cause ionization in the upper atmosphere, thus affecting the density and, consequently, drag. Charges on particles can also alter the attractive forces experienced by the satellite, but this effect is very small and is almost always ignored. In addition, ionization interferes with satellite tracking and communication, and charged particles can interfere with onboard electromagnets that impose torques and perform slow attitude manoeuvers. Since the magnetic field strength varies with the Earth's surroundings, it is usually modelled with a spherical harmonic expansion of low degree and order (exactly analogous to gravitational models) [9]. To measure geomagnetic activity and determine the heat generated, two geomagnetic indices, planetary index k_p and planetary amplitude A_p are used. The former is a quasi-logarithmic, worldwide average of geomagnetic activity below the auroral zones, while the latter is a linear equivalent of the former index, designed to minimize differences at 50° latitude. Both of them are compiled using measurements from twelve observatories which lie between 48° N and 63° S latitudes, but the most accepted compilation of the measurements from these observatories is from the Institut für Geophysik at Göttingen University, Germany [9].

Figure 2.6 shows the daily values of the planetary amplitude from 1986 to 2022, in gamma units, where one gamma equals $10^{-9}\,Tesla$.

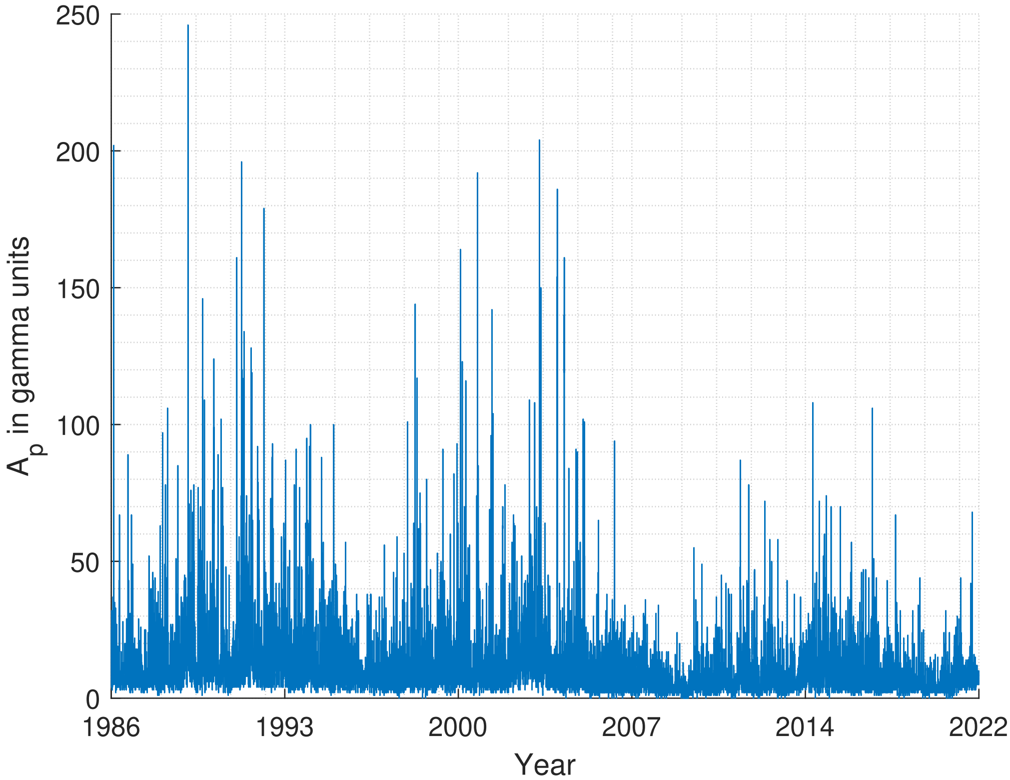

Figure 2.6: A_p daily values over the years

As observed in figure 2.6, A_p has values from 0 to 300, but values greater than 100 are rare, and values of 10–20 are average. A_p daily values tend to follow the 11-year cycle of sunspots, although consistently large maxima of Ap usually occur in the declining phase of each 11-year cycle of $F_{10.7}$. variations are mainly due to solar flares, coronal holes, disappearing solar filaments, and the solar-wind environment near the Earth (Fraser-Smith, 1972).

Eventually, the effects of drag resulting from magnetic disturbances are noticeable for satellites at altitudes between 300 km and 1000 km [9].

The Solar Radiation Pressure

The solar radiation pressure (SRP) effect consists of a force, due to incoming radiation from the Sun, that is exerted on the satellite. In the analysis of SRP, modelling and predicting solar activity is fundamental. In fact, during periods of intense solar activity, the effect of SRP may be more intense than those of the other perturbation, while negligible during low solar activity. In addition, the effect of solar radiation pressure is directly proportional to the altitude.

The relevant aspects in defining the acceleration due to SRP are the determination of the orbital attitude of the satellite, the value of the solar radiation pressure, the determination of the cross-section exposed to incoming radiation and the coefficients modelling the reflectivity of the satellite [9]. Over the cross-sectional area, as for drag, SRP also requires to determine the shadowing effect on the spacecraft. To develop the expression of the acceleration on satellite due to SRP commonly used in numerical analysis, finding the solar pressure, the force due to incoming radiation and then dividing by the mass of the satellite is necessary. Starting with Einstein's law relating energy with mass, $E = mc^2$ and explicating the momentum $m\,c$, the value of solar pressure is obtained:

$$p_{SRP} = \frac{SF}{c} = \frac{1367}{3 \times 10^{-8}} \frac{W/m^2}{m/s} = 4.57 \times 10^{-6} \frac{N}{m^2} \tag{2.24}$$

where SF is the solar-radiation constant and c is the speed of light. SF is a constant approximation of the intensity of the energy of the incoming radiation from the Sun. Many programs use this value or a similar one because determining the actual is challenging and varies over time [9]. In the end, the acceleration due to SRP is defined by the equation 2.25:

$$\ddot{\bar{r}} = -\frac{p_{SRP}\, c_R\, A_\odot}{m} \frac{\bar{r}_{sat\odot}}{r_{sat\odot}} \tag{2.25}$$

where c_r is the reflectivity and $A_\odot$ the exposed area to the Sun. Adopting $\bar{r}_{sat\odot}/r_{sat\odot}$ as a unit vector, the minus sign indicates that the direction of the acceleration on the satellite is always away from the Sun. As far as the c_r, it indicates how the satellite reflects incoming radiation. It has a value between 0.0, i.e. the object is translucent to incoming radiation, and 2.0, i.e. all the radiation is reflected. It is another parameter that varies with time and is difficult to evaluate, especially for complex satellites made of various materials, that enter and exit eclipse regions, and have a constantly changing orientation.

Note that equation 2.25 is an estimation of the actual problem because it is assumed that the surface maintains a constant attitude perpendicular to the Sun. In addition, the reflection process is featured by absorption followed by reflection and the surface can reflect diffusely or mirrorlike with changing aspects toward the Sun. Hence, at any moment, the satellite will experience a net force, not along the Sun-satellite vector, plus a net torque [9]. Due to the interest in orbital motion, often the torque is ignored and $A\odot$ is an average effective cross-section that implicitly incorporates c_R.

Third body and Tides

Supposing m_p and μ_p the mass and the gravitational parameter of the third body respectively, $\bar{R}$ as the distance between the third body and the Earth and $\bar{\rho}$ as the distance between the third body and the satellite, it is obtained the equation 2.26:

$$\ddot{\bar{r}} + \frac{\mu}{r^3}\bar{r} = \mu_p \left(\frac{\bar{R}}{R^3} - \frac{\bar{\rho}}{\rho^3} \right) \tag{2.26}$$

The equation 2.26 is derived as the two-body equation 2.1, thus first considering an inertial frame (**X**,**Y**,**Z**) and a non-rotating frame parallel to the first originating in M, and then studying the relative position, velocity and acceleration in the second, as shown in figure 2.7.

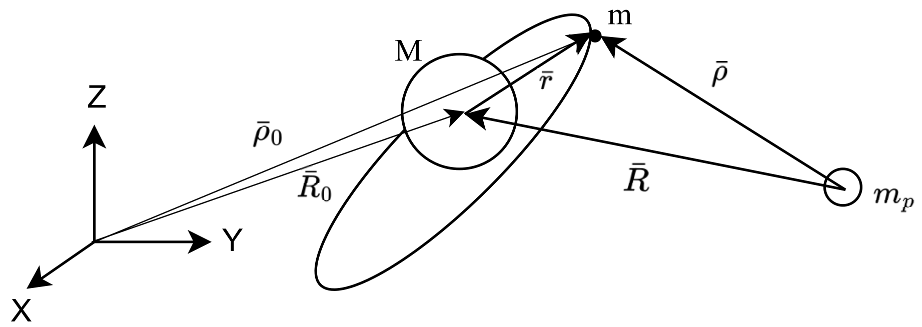

Figure 2.7: Third Body

Note that $\bar{a}_p$, i.e. the perturbative acceleration (the second member of the equation 2.26) acts on the direction connecting the spacecraft to the Earth. Furthermore, the perturbative action results from the difference in the action of the attractive force of the third body on the Earth and the satellite. It also noticed that third bodies, such as the Sun or Moon, have a greater effect on satellites in higher-altitude orbits.

At this point, the third-body's effect on the satellite is determined by integrating numerically equation 2.26. However, considering the disturbing third body is the Sun, the distance from the satellite to the Sun and the distance from the Earth to the Sun are very similar, so $\bar{a}_p$ is very small and may introduce errors during a simulation. Long et al. [13] state this numerical difficulty is not a problem for Earth satellites, but it can be a problem around other central bodies and may produce significant errors for the Moon. Therefore, a different solution has to adopt as using the expansion of Taylor neglecting small terms [13] or Legendre function [14].

As for other perturbative forces, which are often small and negligible, tides are the result of a gravitational distortion caused by an external body (e.g. the Earth, Moon and Sun) [9]. Furthermore, the Earth's rotation introduces periodicity into these effects. Tides include those of the solid Earth as well as those of the oceans. The former are deformations of the Earth due to perturbing forces of external gravitational attraction, in particular the Moon, while the latter cause a large change in mass distribution as water reacts to various gravitational attractions. The accuracy of measurements made with tide gauges (in particular their location is crucial) and human's limited understanding of the world's oceans are the two main problems related to the subject of tides.

Chapter 3

Simulation software

3.1 Systems Tool Kit

The simulation of CubeSat orbital dynamics is performed by STK with an educational license. It is a multiphysics software application from Ansys Government Initiatives (AGI), the US national security subsidiary of Ansys, a world leader in engineering simulation.

STK is a mission modelling and analysis software for space, defence and intelligence systems. It allows analysing of the behaviour of complex systems in their operational environments, within a realistic and dynamic three-dimensional simulation over time.

Concerning STK Space, space platform systems and payloads are modelled, including orbit design and manoeuvre planning for satellite and spacecraft missions. The simulations planned for this thesis were carried out either by working directly with STK's graphical user interface or by integrating STK and MATLAB to automate and visualise the analysis results. Integration takes place via STK's COM interface, sending Connect commands directly to STK without communicating through a port, while results are discussed using STK's reports, graphs and 3D animations. The STK capabilities used in this thesis are:

- Building a Scenario
- Astrogator
- High Precision Orbit Propagator (HPOP)
- Access Tool
- Conjunction Analysis
- Generating Reports and Graphs

The main reference of this chapter is the STK online guide provided by AGI [15].

3.2 Building a Scenario

The scenario is the environment in which a mission is simulated by creating models of systems and evaluating their characteristics and interactions based on physics.

General properties define the scenario, such as analysis period, units of measure, and animation. The definition of units allows all units used in the scenario to be set, including for the period of analysis. The latter is necessary to establish the epoch and the start and end times. The former is a reference for all other times, so the epoch time and date correspond to zero epoch seconds. The seconds, on the other hand, identify the propagation limits of the satellite's orbit.

For each scenario, various objects can be identified for investigation, such as facilities, satellites, aircraft and ground vehicles to instruments such as receivers and transmitters. By selecting the *Insert STK Objects* tool from the insert menu, object properties can be defined, while with *Standard Object database*, the object and its characteristics are downloaded from the local STK database or from the online one. Eventually, reports and other analytical tasks, derived from the scenario information, enable the results of the work for further analysis.

3.3 Astrogator

With regard to the Satellite object with which, in this study, the properties and behaviour of the CubeSats in Earth orbit are modelled, the customized basic property is the *orbit*. This includes defining the orbit propagator and subsequently the coordinate system, orbital elements, and time parameters of the satellite. The STK Astrogator capability is chosen as the orbit propagator, which enables the modelling of impulsive and finite manoeuvers, spacecraft trajectory design and orbit propagation with high fidelity. It calculates satellite ephemeris by executing a Mission Control Sequence (MCS), defined according to mission requirements.

Astrogator also uses a component catalogue and STK editor called *Component Browser*. The latter allows the definition and customization of engine models, force models, propagators, core bodies, atmospheric models and other elements of a space mission analysis scenario. A customized component can be created by duplicating an existing component or by importing one from a file.

3.3.1 Mission Control Sequence

The MCS is a sequence of mission segments that define how Astrogator calculates the spacecraft's trajectory based on the general settings of each segment. It is represented schematically by a tree structure that lists the segments and illustrates their relationships to each other. Segments are generally subdivided into those that generate ephemeris and those that concern the execution of the MCS. Those used in this thesis belong to the first category and are:

Follow The *Follow segment* enables the spacecraft to be attached to another vehicle (the leader) at a certain offset and to be separated when certain conditions occur. In this segment, the offset from the leader's body frame, joining and separation conditions, spacecraft and fuel tank (if any) parameters can be set. The segment adds the specified offset to the ephemeris points of the leader from the fulfilment of the join condition to the fulfilment of the separation condition.

Initial State The *Initial State segment* defines the initial conditions of MCS or of a subsequence within the MCS. In this segment, in addition to the parameters of the spacecraft and the fuel tank (if any), it is possible to set the coordinate system, orbit epoch and orbital elements of the spacecraft. In particular, the orbit epoch is the time when the established elements of the orbit are true. The defined state is added to the ephemeris and passed on to the next segment.

Maneuver The *Maneuver segment* enables to model a finite, impulsive or optimal finite manoeuvre. As for the impulsive manoeuvre, the new state, added to the ephemeris and passed on to the next segment, is calculated by adding a ΔV vector to the velocity of the final state of the previous segment. In contrast, in the case of finite manoeuvre, the state is evaluated as in the *Propagate segment* with the addition of a thrust. Finally, the finite optimal manoeuvre allows the calculation of the thrust attitude and manoeuvre duration to optimise a certain objective function and satisfy a set of constraints, after the selection of the thrust magnitude. Thus, the kind of manoeuvre, the engine model, the attitude, i.e the way to define the manoeuvre-pointing direction, the magnitude of the thrust and the propagator (in case of finite manoeuvre) can be set. Specifically, in the attitude window is possible to describe the direction of acceleration applied to a satellite thanks to the *Thrust vector* command. This direction is opposite to the exhaust of an engine.

Propagate The *Propagate segment* enables the movement of the spacecraft along its current trajectory to be modelled until the specified stopping conditions are reached. In this segment, the stopping conditions and the propagator can be set. The latter is accessible from a list of predefined propagators, but can also be customised from the Component Browser. Over the propagation, each new point of the state is added to the ephemeris. After each step, the stopping conditions are checked. If they are satisfied, the propagation is stopped and the state is passed to the next segment.

Update The *Update segment* is used to change spacecraft properties during propagation. It is possible to replace the parameter value with a new one or subtract and add an entered quantity.

3.4 High Precision Orbit Propagator

A propagator enables the orbit of a satellite to be defined, including the coordinate system, orbital elements and time values as well as propagating the orbit. HPOP generates ephemerides using numerical integration of the differential equations of motion. The choice of HPOP as a propagator also includes the definition of force models, the selection among several perturbation techniques and formulations of the equation of motion.

Usually, it is possible to select and customized HPOP from the *Orbit* properties page of the satellite object. In this thesis, however, it is proceeded from the *Component Browser* page by selecting the *Propagators*. This is the way to use a custom HPOP in the *Propagate* and/or *Maneuver segment* of Astrogator. Satellite's interval and step size (i.e period of analysis, *Orbit Epoch* and *Coordinate Epoch* which specifies the epoch of the input coordinate system), coordinate system, coordinate type, force models, integration methods and covariance (i.e. to propagate the matrix that expresses the uncertainty of the satellite's position and velocity) can be entered with the first method. Instead, from the *Component Browser* is possible to define the integration and the force models, while the other properties are defined in the Astrogator's MCS.

Force modelling involves a full gravitational field model (based upon spherical harmonics), third-body gravity, atmospheric drag, solar radiation pressure and third-body perturbation. Regarding the atmospheric models, the following are selected:

Jacchia-Roberts *Jacchia-Roberts* model computes atmospheric density based on the composition of the atmosphere, which depends on altitude and seasonal variations, using analytical methods to improve performance. The lower altitude boundary is 90 km.

DTM 2012 *DTM 2012* is the 2012 version of the Drag Temperature Model, a semi-empirical model that computes the temperature, density, and composition of the thermosphere. It was developed at CNES and has a valid range of 120 to 1,500 km.

NRLMSISE 2000 *NRLMSISE 2000* is an empirical density model developed by the US Naval Research Laboratory and based on satellite data. It finds the total density by accounting for the contribution of N, N2, O, O2, He, Ar and H. It includes anomalous oxygen. This 2000 version has a valid range of 0 to 1,000 km.

Atmospheric models are closely related to the solar flux and geo-magnitude values. Constant values or data files can be entered. As seen in subsection 2.3.3, the flux file contains the data A_p, k_p, $F_{10.7}$ and the average of $F_{10.7}$ for each date. STK reads the geomagnetic flux data, A_p and k_p from a file and each density model uses the appropriate data natively. The files used in this thesis are *SpaceWeather.txt* and *SolarFluxCSSI.dat*. The first one is available on the Celestrak website [16] and sponsored by CSSI and AGI. It contains daily observed solar flux and geomagnetic indices, and approximately ten years of predicted data. For geomagnetic flux data, a daily value and eight values measured at three-hour intervals for each date are included. Moreover, it contains an observed $F_{10.7}$ value and one adjusted to 1 AU, obtained with the equation 2.23.

SolarFluxCSSI.dat is an ASCII file used for long-term forecasts. The file contains the predicted values of the monthly average of $F_{10.7}$ and the geomagnetic index, A_p in UTC. The file consists of a first line with seven numbers describing the data limits and the remaining lines containing the forecasts. Specifically, the first line contains the year and month in which the data begin and end, the year and month in which the predictions were generated, and the number of points that follow. Each of the remaining rows, instead, assuming the day to be the 15^{th} of the month, contains the year and month, followed respectively by the +2s and nominal forecasts of $F_{10.7}$ and the +2s and nominal forecasts of A_p. Taking into account the +2s value means to consider the nominal solar flux plus the product of the solar flux sigma level and the standard deviation σ associated with the nominal solar flux value.

With regard to the gravity model, it enables configuring a central body gravity model, solid and ocean tide effects, and third body gravity effects. The effect of the Moon and Sun as the third body perturbation and EGM2008 as the gravity field file are the STK default inputs. In the *Gravitational Force* menu, it is possible to include the perturbation of the gravity field caused by the effects of solid tides, using the solid-tide model available for the Central Body. It is possible to exclude this contribution, consider only the permanent ones or take them all into account. It is also possible to select *Truncate to Gravity Field Size* to exclude the solid tide terms beyond the degree and order selected for the gravity model itself and to select *Use Ocean Tides*. By default, 21 is the order and degree for the gravity model, while the options *Truncate to Gravity Field Size* and *Permanent tide only* are selected, but not *Use Ocean Tides*.

Modelling SRP consists of selecting the shadow model, the sun position type, the eclipsing body and the atmospheric altitude for the eclipse. A shadow model allows selecting the level of precision to compute the reduction in solar radiation pressure caused by an eclipsing body as it obscures the sun. By default, the dual cone model uses the actual size and distance of the Sun to model regions of full, partial (penumbra), and zero (umbra) sunlight. The visible fraction of the solar disk is used to compute SRP during penumbra. The primary central body is always considered an eclipsing body except for the case where the primary central body is the Sun. The Moon, instead, is the default extra-central body. Computing the Sun position means identifying the direction of the Sun for SRP computations. By default, *Apparent Sun to True CB* is selected. It takes into account the time required for light to travel from the sun to the central body. By default, STK uses the Earth's surface shape, which corresponds to an atmospheric altitude of 0 km. Thus, attenuation and refraction of solar radiation through the atmosphere are not accounted for.

Finally, the integrator model allows the selection of the integration method, step size control, interpolation method and other functions related to the chosen integration method. RKF 7(8) is the STK's default integration method of 7th order with 8th order error control for the integration step size. The step size control can be *Fixed Step* i.e. the step size remains constant throughout the integration of the orbit and no error control is used or *Relative Error* i.e. the step size control is based on the relative error by providing the error tolerance and the minimum and maximum integration step size to be allowed by the relative error control. Among the possible interpolation methods is the Lagrange interpolation method, which uses the standard Lagrange interpolation scheme, interpolating position and velocity separately; it is also possible to specify the order of interpolation. Alternatively, a Hermitian interpolation scheme can be selected, which uses position and velocity ephemerides to interpolate position and velocity together (i.e., using a polynomial and its derivative). It is also possible to specify the interpolation order. In addition, a propagation stop is possible if any sample of the force model occurs at an altitude less than this specified value.

3.5 Access Tool

The *Access Tool* allows determining when an object can *access* or see another object. Furthermore, valid accesses can be identified by imposing constraints as properties on the objects between which accesses are calculated. It is possible to calculate the accesses of all types of vehicles, structures, area targets and sensors to all objects within a scenario.

Access is defined by two objects, a primary object and an associated object, for which STK computes the access. The access created maintains a close relationship with the defining objects. If the definition objects are removed from the scenario or one of them changes in a way that alters the access times, STK automatically removes the access data or recalculates it, respectively.

The Access Tool models also signal transmission between the two objects. Usually, STK will consider light time delay between the objects but will only consider aberration in certain circumstances. Moreover, it can compute accesses to an entire group of assets using the *Chain object*. The latter object enables the assignment of objects to the chain and defines the order in which the objects are accessed.

With the *Access Tool* it is possible to generate a report or graph providing access times between the primary object and one or more selected objects. In addition, an access report or graph can be generated with azimuth (Az), elevation (El) and range data. Displayed data are for valid access periods. On the other hand, the azimuth and elevation values are calculated based on the local coordinate system of the object for which the access window is displayed. As far as satellites, it is the Vehicle Velocity Local Horizontal (VVLH) which consists of three axes in the Earth's Inertial reference system aligned and constrained to position and velocity vectors along the trajectory of the point (the satellite) relative to the reference system. Specifically, the Z-axis is opposite to the position vector and X-axis is toward the inertial velocity vector. El is measured toward negative Z. Figure 3.1 shows the VVLH coordinate system and how azimuth and elevation are defined in it.

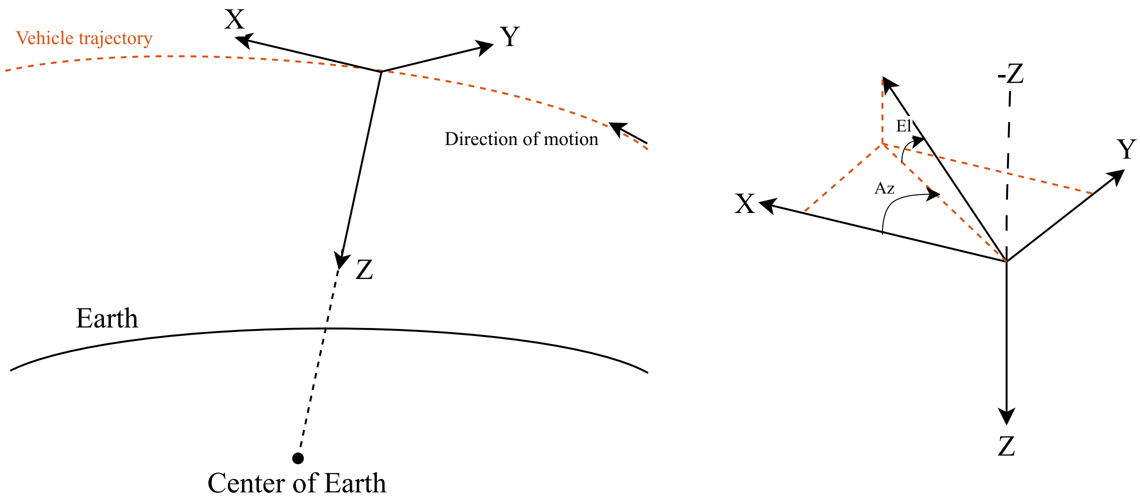

Figure 3.1: VVLH coordinate system

Chapter 4

Simulation properties

4.1 Nominal simulation parameters

4.1.1 Satellite modelling

The simulations performed involve CubeSats deployed from the ISS. Single-unit, double-unit and triple-unit CubeSats are considered. Their nominal physical features are summarised in table 4.1 while figure 4.1 shows the process of evaluating the average area adopted by the CROC tool.

Table 4.1: CubeSat nominal properties

CubeSat	**Size**	**m**	**XA**	C_D	**Attitude**
1U	$10^2 \cdot 10$ cm^3	1 kg	0.0148 m^2	2.2	tumbling
2U	$10^2 \cdot 20$ cm^3	2 kg	0.0247 m^2	2.2	tumbling
3U	$10^2 \cdot 30$ cm^3	3 kg	0.0346 m^2	2.2	tumbling

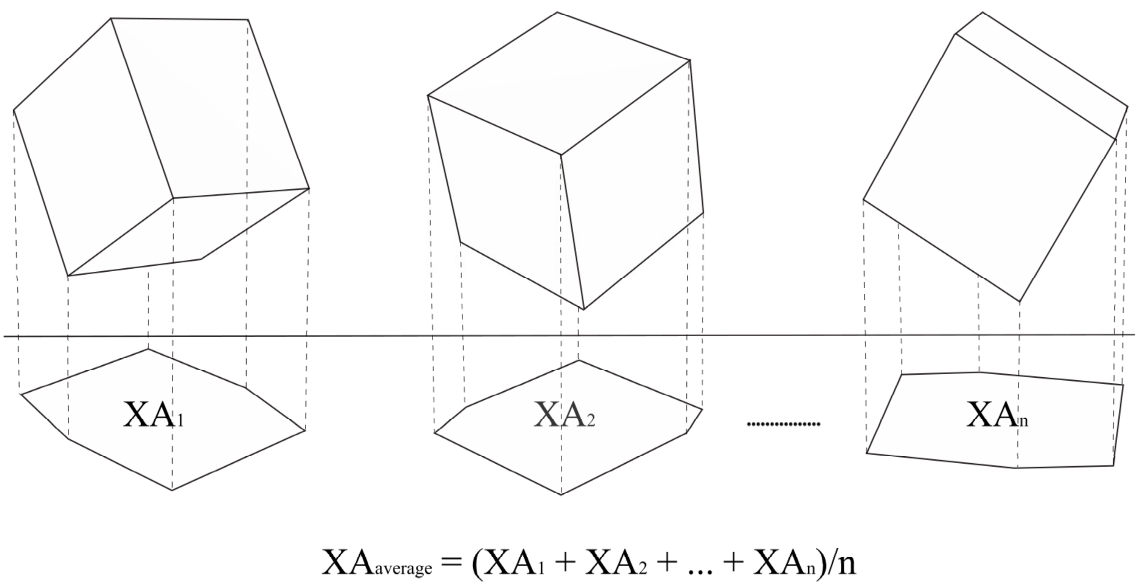

Figure 4.1: Cross-sectional area estimation process

As shown in figure 4.2, the simplest versions of CubeSats are chosen, so a cube with an edge of 10 cm and two parallelepipeds with a base of 10 cm and a height of 20 cm and 30 cm respectively are entered in the CROC tool as satellite models. They could be a good approximation of real CubeSats with body-mounted solar panels and small antennas.

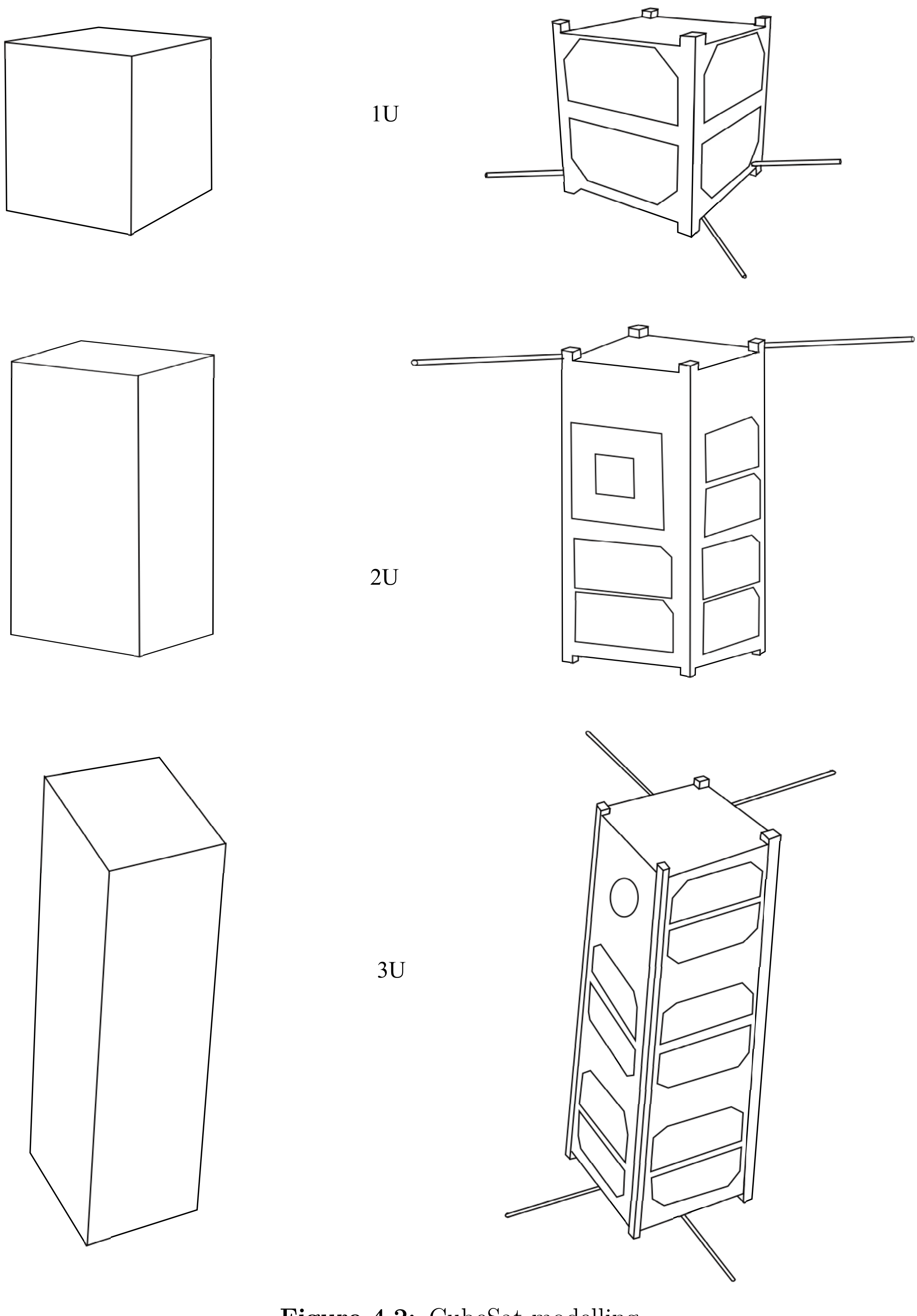

Figure 4.2: CubeSat modelling

Regarding CubeSat nominal properties, typical values of size, mass and CD are assumed, while the CROC tool of ESA's open-source software Drama is used to estimate the average cross-sectional area of satellites. In the analyses of this thesis, the way adopted to simulate a specific attitude of the satellite is to vary the value of the input cross-sectional area. With regard to the nominal attitude, it is assumed that the satellites rotate randomly around their body axes after deployment so an average area as a drag area is suitable for analyses. This area is calculated by the CROC tool by averaging the flat projections of the satellites for each of their possible space orientation (figure 4.1).

4.1.2 Epoch and classical orbital elements of the ISS

Time data are expressed in gregorian UTC (UTCG). 1^{th} October 2022 12:00:00.000 UTCG is selected as the default start time of the simulations. At this instant, the orbital elements of the ISS are those highlighted in table 4.2. The ISS data are downloaded by STK thanks to the function *Standard Object database* (explained section 3.2), which provides access to the satellite database updated by the U.S. Strategic Command (USSTRATCOM) [15].

Table 4.2: Orbital elements of the ISS

Subject	**a**	**e**	**i**	$\boldsymbol{\Omega}$	$\boldsymbol{\omega}$	$\boldsymbol{\nu}$
ISS	6798 km	0.0013	51.68°	169°	60.8°	323°

4.1.3 General features of Astogator's MCS

The *Follow segment* and the *Maneuver segment* are added to the MCS to fully model the release of satellites from the ISS. In the first one, the ISS is chosen as *Leader Vehicle*, while the position of the CubeSat with respect to the leader's body frame is represented by the X, Y and Z distances:

$$\begin{cases} X = 0.006 \ \ km \\ Y = -0.014 \ \ km \\ Z = 0.008 \ \ km \end{cases}$$

This point is a good approximation of the point at which, in the ISS extravehicular environment, the JEMRMS transports the NRCSD from the pressurised volume to deploy the satellites. The *Joining conditions*, the *Separation conditions* and the *Spececraft parameters* to enter in the segment, instead, are defined according to the type of simulation.

Regarding the ΔV of deployment, i.e the impulse provided by the deployer to the CubeSat, in the *Maneuver segment* an impulsive manoeuvre is selected and choosing *Thrust Vector* in the attitude control window, the thrust is defined in spherical coordinates. VVLH are the thrust axes while Az, El and magnitude are the spherical coordinates:

$$\begin{cases} Az = 180° \\ El = 45° \\ Magnitude = 1.5 \ \ m/s \end{cases}$$

These values are chosen to simulate a nominal deployment where the NRSCD points 45° downwards and in the opposite direction to the motion of the ISS. Figure 4.3 is a representation of the direction of the thrust imparted to the CubeSat in the VVLH coordinate system, while figure 4.4 shows the position of the CubeSat at the beginning of the simulation on STK.

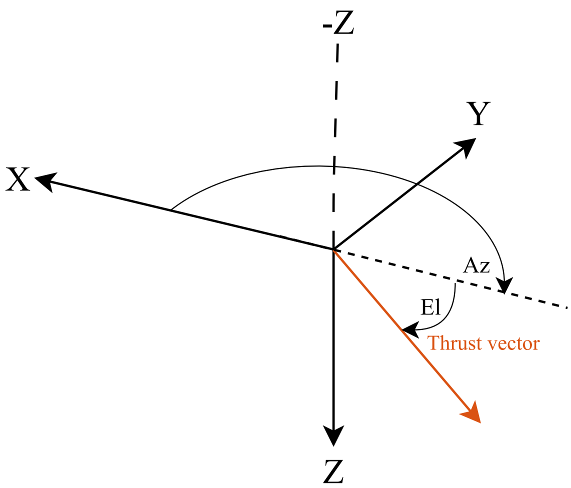

Figure 4.3: Thrust Vector

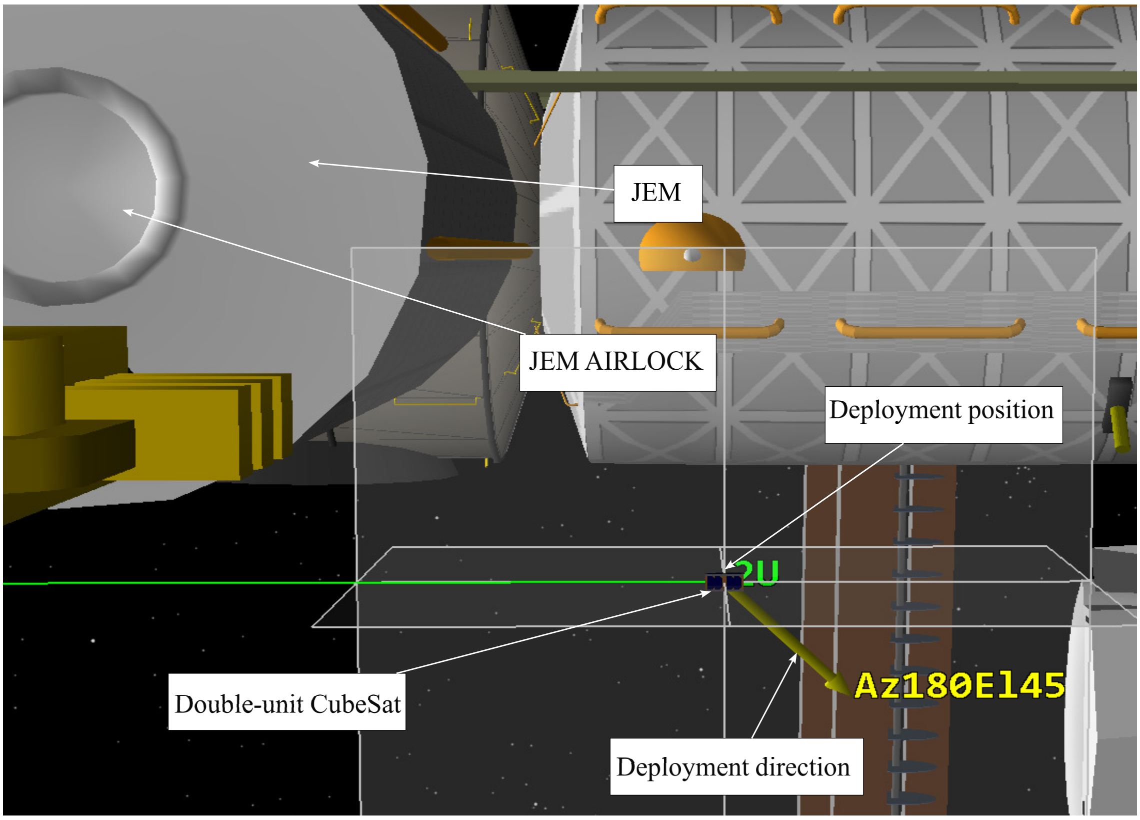

Figure 4.4: Deployment position on STK

As shown in figure 4.4, the yellow vector indicates the direction of deployment (i.e. the thrust vector in figure 4.3) and the green line the orbit. Furthermore, the image of the CubeSat is only a cad model loaded to represent its dimensions, but STK only propagates the mass point and therefore the figure also represents the starting point of propagation (i.e. the deployment position).

As far as the orbit propagation, two stop conditions are defined in the *Propagate segment*. The first is a duration of 3 years, whereas the second is an altitude of 120 km above the central body. Moreover, HPOP, which is customised in the *Component Browser* according to the type of simulation, is chosen as the propagator for this segment. The nominally HPOP consist of STK default models of the gravitational force and spherical SRP, while *NRLMSISE 2000* is chosen as the atmospheric model and *SpaceWeather.txt* as the solar flux file. The influences of the Moon and the Sun are taken into account. In addition, the integration method is RKF 7(8) and an initial and minimum step of 300 s and 350 s respectively are selected. Finally, when it is not possible to simulate a complete deployment due to the lack of ISS TLE, an *Initial State segment* is necessary. In this case, the ISS orbital parameters (table 4.2) are chosen as CubeSat ones while the deployment date and time as the *Orbit Epoch*.

4.2 Preliminary analysis

First, the effect of the satellite's position along its orbit on its lifetime is studied. Subsequently, the variation of the longitude of the ascending node is also considered. Tables 4.3 and 4.4 show the relevant inputs of the simulation of the position in orbit and of the variation of the Ω, respectively.

Table 4.3: Inputs for the orbit position study

Parameter	**Value**		
Scenario Epoch	1^{st} October 2022 12:00:00.000 UTCG		
MCS segments	*Follow*, *Maneuver* and *Propagate*		
Follow segment			
Leader Vehicle	ISS		
Offset from leader	X=6 m, Y=-14 m, Z=8 m		
Joining Conditions	1^{st} October 2022 12:00:00.000 UTCG		
Sep. Conditions	ν=0°, 60°, 120°, 180°, 240°, 300°, 360°		
Fuel tank	engines and tanks not planned		
Satellite	**1U**	**2U**	**3U**
m	1 kg	2 kg	3 kg
XA	0.0148 m^2	0.0247 m^2	0.0346 m^2
C_D	2.2	2.2	2.2
Maneuver segment			
Type of Maneuver	Impulsive		
Thrust axes	VVLH		
Thrust Vector	Az=180°, El=45°, $\|\Delta V\|$=1.5 m/s		
Propagate segment			
Propagator	HPOP		
Density model	*NRLMSISE 2000*		
Solar flux file	*SpaceWeather.txt*		
Stop condition 1	Duration of 3 years		
Stop condition 2	Altitude of 120 km		

Table 4.4: Inputs for the Ω study

Parameter	Value		
Scenario Epoch	1^{st} October 2022 12:00:00.000 UTCG		
MCS segments	*Initial State*, *Maneuver* and *Propagate*		
Initial State segment			
Orbit Epoch	1^{st} October 2022 12:00:00.000 UTCG		
Fuel tank	engines and tanks not planned		
a	6798 km		
e	0.0013		
i	51.68°		
Ω	0°, 60°, 120°, 180°, 240°, 300°, 360°		
ω	60.8°		
ν	324°		
Satellite	**1U**	**2U**	**3U**
m	1 kg	2 kg	3 kg
XA	0.0148 m^2	0.0247 m^2	0.0346 m^2
C_D	2.2	2.2	2.2
Maneuver segment			
Type of Maneuver	Impulsive		
Thrust axes	VVLH		
Thrust Vector	Az=180°, El=45°, $\|\Delta V\|$=1.5 m/s		
Propagate segment			
Propagator	HPOP		
Density model	*NRLMSISE 2000*		
Solar flux file	*SpaceWeather.txt*		
Stop condition 1	Duration of 3 years		
Stop condition 2	Altitude of 120 km		

The scenario epoch is the 1^{st} October 2022, while the satellite features are those highlighted in table 4.1.

As far as the position study, the Astrogator's MCS consist of the *Follow*, *Maneuver* and *Propagate segments*. In the *Follow segment*, the ISS is selected as the *Leader Vehicle*, whereas the ν of the CubeSats as *Separation conditions* and its value is overridden by automating with MATLAB. In this way, during propagation, when the ISS reaches the position in orbit corresponding to the specified value of ν, the CubeSat is deployed from the ISS. In the second segment, the default manoeuvre is defined as described in subsection 4.1.3, while the nominal HPOP and *Stopping conditions* are entered in the *Propagator segment*.

Concerning the Ω analysis, the Astrogator's MCS consist of *Initial State*, *Maneuver*, and *Propagate segments*. In this case, it is not possible to use the *Follow segment* because, on the date of deployment, the Ω of the ISS is equal to the value indicated in table 4.2 and cannot be changed. As a consequence, the *Initial State segment* is chosen to define the CubeSat properties. The orbital parameters are chosen the same as the ISS in table 4.2 while the value of the Ω is varied. In the second segment, the default manoeuvre is defined as described in subsection 4.1.3, while the nominal HPOP and *Stopping conditions* are entered in the *Propagator segment*.

4.3 Deployment altitude

Since the birth of the ISS, the altitude of the orbiting Space Station has changed continuously. The ISS trajectory is subject to perturbative actions such as resistance due to the Earth's atmosphere reducing its altitude. To compensate for this, the Space Station receives periodic boosts. Figure 4.5 shows the average altitude of the ISS over the years, obtained using the definition of mean motion (equation 2.9) contained in the TLE of the ISS provided by CeleStrack, and the orbital period equation (equation 2.6). In particular, an Earth radius of 6378 km is considered and the altitude is calculated by subtracting this value from the semi-major axis of the ISS. Based on the values obtained, the purpose of the *Deployment altitude analysis* is to understand how the variation in ISS altitude can affect the lifetime of CubeSats.

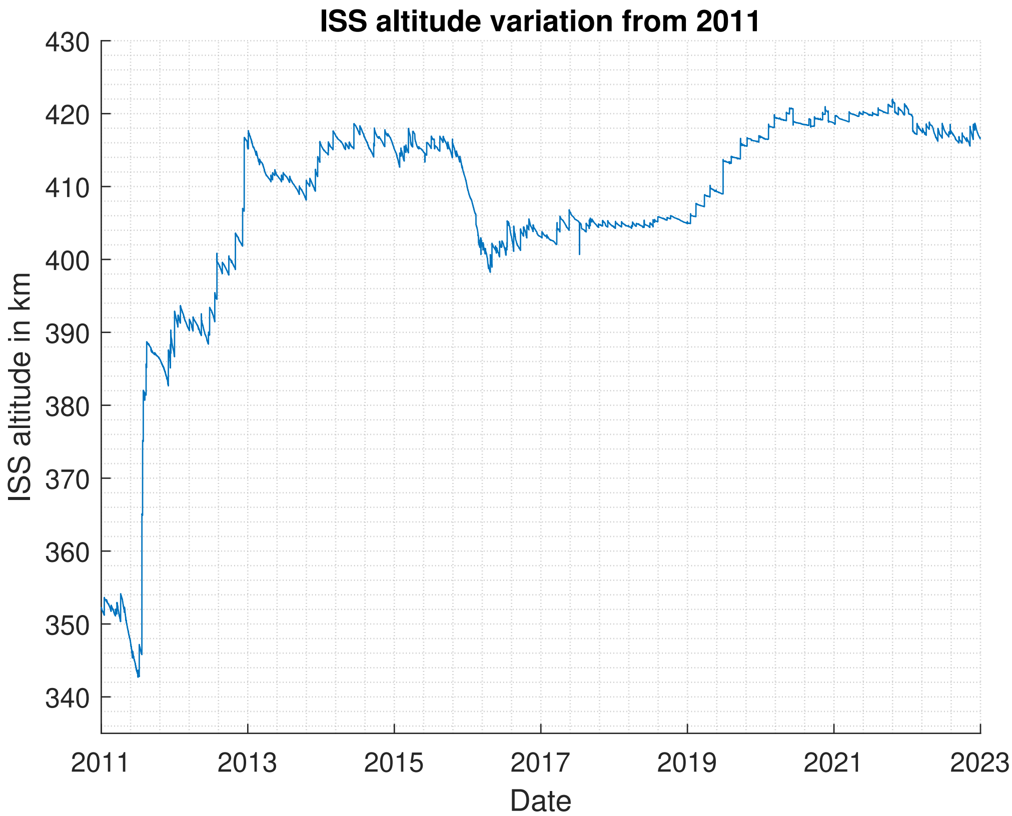

Figure 4.5: ISS altitude over the years

The date of deployment is 1^{st} October 2022. The Astrogator's MCS is composed of the *Initial State*, *Maneuver* and *Propagate* segments. In the first segment, the nominal parameters of the satellites (table 4.1), their orbital elements (chosen equal to those in table 4.2) and the *Orbit Epoch* are entered. Particularly, the value of the semi-major axis is overridden by automating with MATLAB. The a value is calculated supposing an Earth radius of 6378 km. In this case, it is not possible to use the *Follow segment* because, on the date of deployment, the a of the ISS is equal to 6798 km (table 4.2) and it cannot be changed. With regard to the *Maneuver segment* the nominal parameters as described in subsection 4.1 are selected. The same is true for those in *Propagate segment* with the exception of the atmospheric density model which is overridden by automating with MATLAB. The models selected are

Jacchia-Roberts, *DTM 12* and *NRLMSISE 2000*. Table 4.5 shows the relevant inputs of the simulation.

Table 4.5: Inputs first simulation

Parameter	Value		
Scenario Epoch	1^{st} October 2022 12:00:00.000 UTCG		
MCS segments	*Initial State*, *Maneuver* and *Propagate*		
Initial State segment			
Orbit Epoch	1^{st} October 2022 12:00:00.000 UTCG		
Fuel tank	engines and tanks not planned		
a	6738→6818 km		
e	0.0013		
i	51.68°		
Ω	169°		
ω	60.8°		
ν	324°		
Satellite	**1U**	**2U**	**3U**
m	1 kg	2 kg	3 kg
XA	0.0148 m^2	0.0247 m^2	0.0346 m^2
C_D	2.2	2.2	2.2
Maneuver segment			
Type of Maneuver	Impulsive		
Thrust axes	VVLH		
Thrust Vector	Az=180°, El=45°, $\|\Delta V\|$=1.5 m/s		
Propagate segment			
Propagator	HPOP		
Density model	*NRLMSISE 2000*, *DTM 12*, *Jacchia-Roberts*		
Solar flux file	*SpaceWeather.txt*		
Stop condition 1	Duration of 3 years		
Stop condition 2	Altitude of 120 km		

4.4 Deployment date

The *Deployment date analysis* consists of changing the day of deployment and comparing the effect of two different solar flux files on the decay time. In particular, the purpose of this simulation is to understand how solar activity influences CubeSat's time in orbit.

Also in this simulation, *Follow segment* is not chosen due to the impossibility to foresee the future TLEs of the ISS. Therefore, the Astrogator's MCS is composed of the *Initial State*, *Maneuver* and *Propagate* segments. In the first segment, the nominal parameters of the satellites (table 4.1) and the orbital elements (chosen equal to those in table 4.2) are entered. Moreover, the value of the *Orbit Epoch* is overridden by automating with MATLAB, to simulate the CubeSat deployment in subsequent years. Therefore, the year of the chosen dates increases by one at a time from 2022 until 2030, while the day and month remain the 1^{st} October. The *Maneuver segment* has the nominal features as described in section 4.1, while in the

Propagate segment after entering the nominal propagator, density model and *Stopping conditions*, two solar flux files from the STK's default data, *SolarFluxCSSI.dat* and *SpaceWeather.txt*, are overridden by automating with MATLAB. Table 4.6 shows the relevant inputs of the simulation.

Table 4.6: Inputs second simulation

Parameter	Value		
Scenario Epoch	1^{st} October 2022 12:00:00.000 UTCG		
MCS segments	*Initial State*, *Maneuver* and *Propagate*		
Initial State segment			
Orbit Epoch	1^{st} October 2022→2030 12:00:00.000 UTCG		
Fuel tank	engines and tanks not planned		
a	6798 km		
e	0.0013		
i	51.68°		
Ω	169°		
ω	60.8°		
ν	324°		
Satellite	**1U**	**2U**	**3U**
m	1 kg	2 kg	3 kg
XA	0.0148 m^2	0.02470.0148 m^2	0.03460.0148 m^2
C_D	2.2	2.2	2.2
Maneuver segment			
Type of Maneuver	Impulsive		
Thrust axes	VVLH		
Thrust Vector	Az=180°, El=45°, $\|\Delta V\|$=1.5 m/s		
Propagate segment			
Propagator	HPOP		
Density model	*NRLMSISE 2000*		
Solar flux file	*SpaceWeather.txt*, *SolarFluxCSSI.dat*		
Stop condition 1	Duration of 3 years		
Stop condition 2	Altitude of 120 km		

4.5 Parametric study

The *Parametric study* involves the estimation of the CubeSats lifetime by varying the elements that make up the ballistic coefficient. In addition, it varies the ΔV of deployment also.

In this analysis, the deployment from the ISS is completely simulated. Astrogator's MCS, in fact, consist of *Follow*, *Maneuver* and *Propagate* segments. In the first segment, ISS is selected as *Leader Vehicle* while the *Joining condition* is the epoch of the scenario, the 1^{st} October 2022. By automating with Matlab, the element constituting the β, and the $|\Delta V|$ of deployment are overridden as many times as the number of inputs in the satellite properties window (in the *Follow segment*) and in the *Manoeuvre* segment window respectively. Tables 4.7 shows the main inputs in the Astogrator's segments, while table 4.8 shows the different cases analysed in this simulation.

Table 4.7: Inputs third simulation

Parameter	Value
Scenario Epoch	1^{st} October 2022 12:00:00.000 UTCG
MCS segments	*Follow*, *Maneuver* and *Propagate*
Follow segment	
Leader Vehicle	ISS
Offset from leader	X=6 m, Y=-14 m, Z=8 m
Joining Condition	1^{st} October 2022 12:00:00.000 UTCG
Sep. Condition	1 s
Fuel tank	engines and tanks not planned
Maneuver segment	
Type of Maneuver	Impulsive
Thrust axes	VVLH
Thrust Vector	Az=180°, El=45°, |ΔV|=1.5 m/s
Propagate segment	
Propagator	HPOP
Density model	*NRLMSISE 2000*
Solar flux file	*SpaceWeather.txt*
Stop condition 1	Duration of 3 years
Stop condition 2	Altitude of 120 km

Table 4.8: Cases of the third simulation

Parameter	First case	Second case	Third case	Fourth case
1U				
C_D	1.8→3	2.2	2.2	2.2
XA	148 cm^2	100→190 cm^2	148 cm^2	148 cm^2
m	1 kg	1 kg	0.8→2.4 kg	1 kg
|ΔV|	1.5 m/s	1.5 m/s	1.5 m/s	0.3→2.5 m/s
2U				
C_D	1.8→3	2.2	2.2	2.2
XA	247 cm^2	100→328 cm^2	247 cm^2	247 cm^2
m	2 kg	2 kg	1.8→3.6 kg	2 kg
|ΔV|	1.5 m/s	1.5 m/s	1.5 m/s	0.3→2.5 m/s
3U				
C_D	1.8→3	2.2	2.2	2.2
XA	346 cm^2	100→477 cm^2	346 cm^2	346 cm^2
m	3 kg	3 kg	2.8→4.8 kg	3 kg
|ΔV|	1.5 m/s	1.5 m/s	1.5 m/s	0.3→2.5 m/s

Four cases are defined and in each of them one of the four parameters, CD, XA, m or |ΔV| is varied while the others are fixed. The range of mass variation respects the limits imposed by the NRCSD [3]. On the other hand, |ΔV| is varied between the value imposed by [17] a plus to study other intervals. As for *XA*, a range is chosen with extremes the minimum value estimated by the CROC tool and the maximum value plus ten per cent to simulate possible appendages. Finally, the C_D value varies between the typical values for these categories of satellites [5].

4.6 Drag sail

In this simulation, the effects of deploying a passive de-orbit system, specifically a drag sail, on the time of decay of a 3U are studied.

Table 4.9: Inputs fourth simulation

Parameter	**Value**
Scenario Epoch	1^{st} October 2029 12:00:00.000 UTCG
MCS segments	*Initial State*, *Maneuver* and *Propagate*
Initial State segment	
Orbit Epoch	1^{st} October 2029 12:00:00.000 UTCG
Fuel tank	engines and tanks not planned
a	6798 km
e	0.0013
i	51.68°
Ω	169°
ω	60.8°
ν	324°
Satellite	**3U**
m	3 kg
XA	0.0346 m^2
C_D	2.2
Maneuver segment	
Type of Maneuver	Impulsive
Thrust axes	VVLH
Thrust Vector	Az=180°, El=45°, $\|\Delta V\|$=1.5 m/s
First Propagate segment	
Propagator	HPOP
Density model	*NRLMSISE 2000*
Solar flux file	*SpaceWeather.txt*
Stop condition 1	Duration of 3 years
Stop condition 2	Altitude of 360 km, 370 km, 380 km, 390 km, 400 km
Update segment	
New XA	0.1 m^2, 0.25 m^2, 0.5 m^2, 0.75 m^2, 1 m^2
Second Propagate segment	
Propagator	HPOP
Density model	*NRLMSISE 2000*
Solar flux file	*SpaceWeather.txt*
Stop condition 1	Duration of 3 years
Stop condition 2	Altitude of 120 km

1^{st} October 2029 is chosen as the deployment date of the satellite. This year is expected a minimum solar activity according to the solar flux files of STK. Therefore, it could be interesting to note how to reduce the satellite's time in orbit during this period, exploiting the deployment of a drag sail.

The Astrogator's MCS is sequentially composed of *Initial State*, *Maneuver*, *Propagate*, *Update* and *Propagate segment*. In the first segment the nominal CubeSat properties (table 4.1) and orbital elements (chosen equal to those in table 4.2) and the *Orbit Epoch* are entered. In the second one, the default manoeuvre is defined as described in subsection 4.1.3, while the first *Propagate segment* is used to select at which altitude to deploy the drag sail. The latter datum is overridden by automating with MATLAB. The *Update segment* enables to modify the spacecraft parameters. In this simulation, the value of *XA* is changed defining a new one. Particularly, it is assumed that after the deployment of the drag sail, the CubeSat assumes a minimum drag attitude. As a consequence, the drag sail area corresponds to the new value of *XA*. Finally, in the second *Propagate segment* are entered the nominal propagator and *Stopping conditions*.

4.7 Deployment direction

Finally, the effect of changing the deployment direction is studied. From section 1.2, the nominal direction for satellite deployment is at 45° in the direction opposite to the ISS movement and downwards. This choice is motivated by safety reasons. To implement the STK study, the coordinates of the *Thrust Vector* are changed. As described in subsection 4.1.3, Az, El and magnitude are required to define the *Thrust Vector*. First, a simulation is run in which the values of magnitude and El are taken as nominal, 45° and 1.5 m/s respectively, while Az is varied. Figure 4.6 shows the vectors of some deployment directions implemented in this first simulation. The CubeSat is positioned at its deployment point (defined in line six of table 4.10), while the yellow vector represents the direction in which the CubeSat is released.

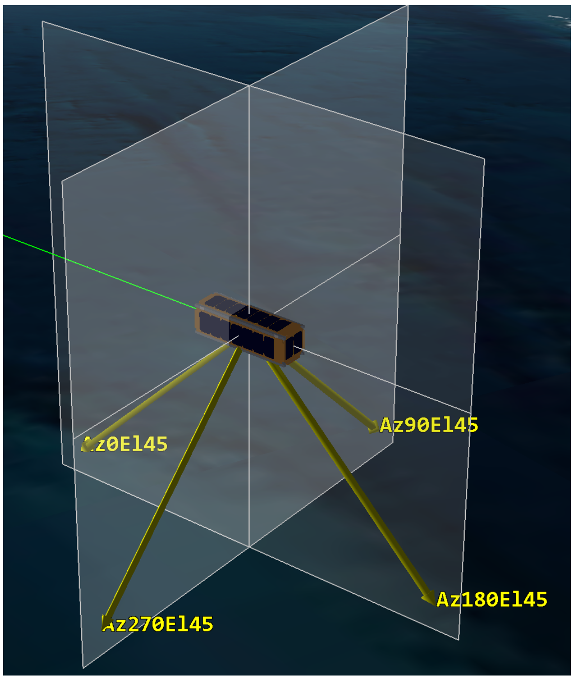

Figure 4.6: Deployment direction with El=45°

In a second simulation, however, El is kept equal to 0° as Az is varied. Figure 4.7 shows 4 of the deployment directions implemented in this second simulation.

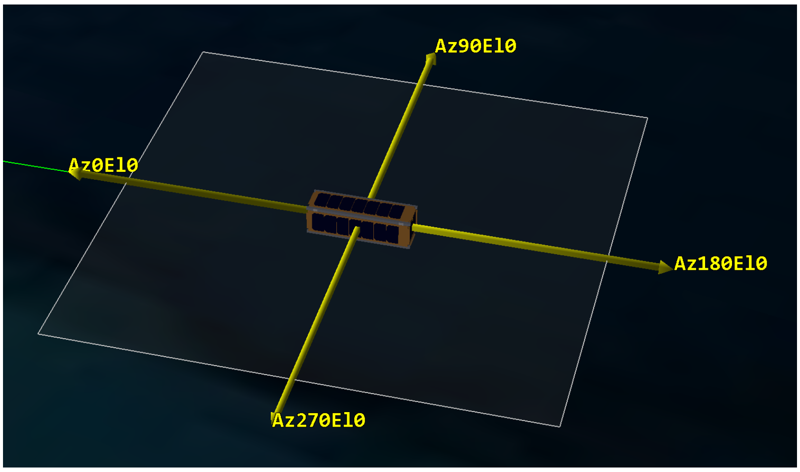

Figure 4.7: Deployment direction with El=0°

Tables 4.10 and 4.11 highlight the main inputs of the two simulations of this section.

Table 4.10: Inputs for first analysis on deployment direction

Parameter	**Value**		
Scenario Epoch	1^{st} October 2022 12:00:00.000 UTCG		
MCS segments	*Follow*, *Maneuver* and *Propagate*		
Follow segment			
Leader Vehicle	ISS		
Offset from leader	X=6 m, Y=-14 m, Z=8 m		
Joining Conditions	1^{st} October 2022 12:00:00.000 UTCG		
Fuel tank	engines and tanks not planned		
Satellite	**1U**	**2U**	**3U**
m	1 kg	2 kg	3 kg
XA	0.0148 m^2	0.0247 m^2	0.0346 m^2
C_D	2.2	2.2	2.2
Maneuver segment			
Type of Maneuver	Impulsive		
Thrust axes	VVLH		
Thrust Vector	Az=0°→315°, El=45°, $\lvert\Delta V\rvert$=1.5 m/s		
Propagate segment			
Propagator	HPOP		
Density model	*NRLMSISE 2000*		
Solar flux file	*SpaceWeather.txt*		
Stop condition 1	Duration of 3 years		
Stop condition 2	Altitude of 120 km		

The Astrogator's MCS is sequentially composed of *Follow*, *Maneuver* and *Propagate segment*. In the *Follow segment*, the ISS is selected as the *Leader Vehicle* while the nominal HPOP and *Stopping conditions* are entered in the *Propagator segment*.In the second segment, following the definition of the manoeuvre in subsection 4.1.3, the impulsive manoeuvre, the VVLH system and the spherical coordinates are selected. While the value of El is set at 45°, the value of Az is overwritten with MATLAB from 0° to 315°. In the same way, the second analysis is set up, but in contrast, the value of El is fixed at 0°.

Table 4.11: Inputs for the second analysis on deployment direction

Parameter	**Value**		
Scenario Epoch	1^{st} October 2022 12:00:00.000 UTCG		
MCS segments	*Follow*, *Maneuver* and *Propagate*		
Follow segment			
Leader Vehicle	ISS		
Offset from leader	X=6 m, Y=-14 m, Z=8 m		
Joining Conditions	1^{st} October 2022 12:00:00.000 UTCG		
Fuel tank	engines and tanks not planned		
Satellite	**1U**	**2U**	**3U**
m	1 kg	2 kg	3 kg
XA	0.0148 m^2	0.0247 m^2	0.0346 m^2
C_D	2.2	2.2	2.2
Maneuver segment			
Type of Maneuver	Impulsive		
Thrust axes	VVLH		
Thrust Vector	Az=0°→315°, El=0°, $\lvert\Delta V\rvert$=1.5 m/s		
Propagate segment			
Propagator	HPOP		
Density model	*NRLMSISE 2000*		
Solar flux file	*SpaceWeather.txt*		
Stop condition 1	Duration of 3 years		
Stop condition 2	Altitude of 120 km		

Chapter 5

Results

5.1 Preliminary analysis

According to the simulation, varying the ν, i.e the CubeSat position relative to the perigee along the orbit, does not affect the lifetime. Figures 5.1 show how the CubeSat's time in orbit changes as the ν value varies depending on the size of the satellites.

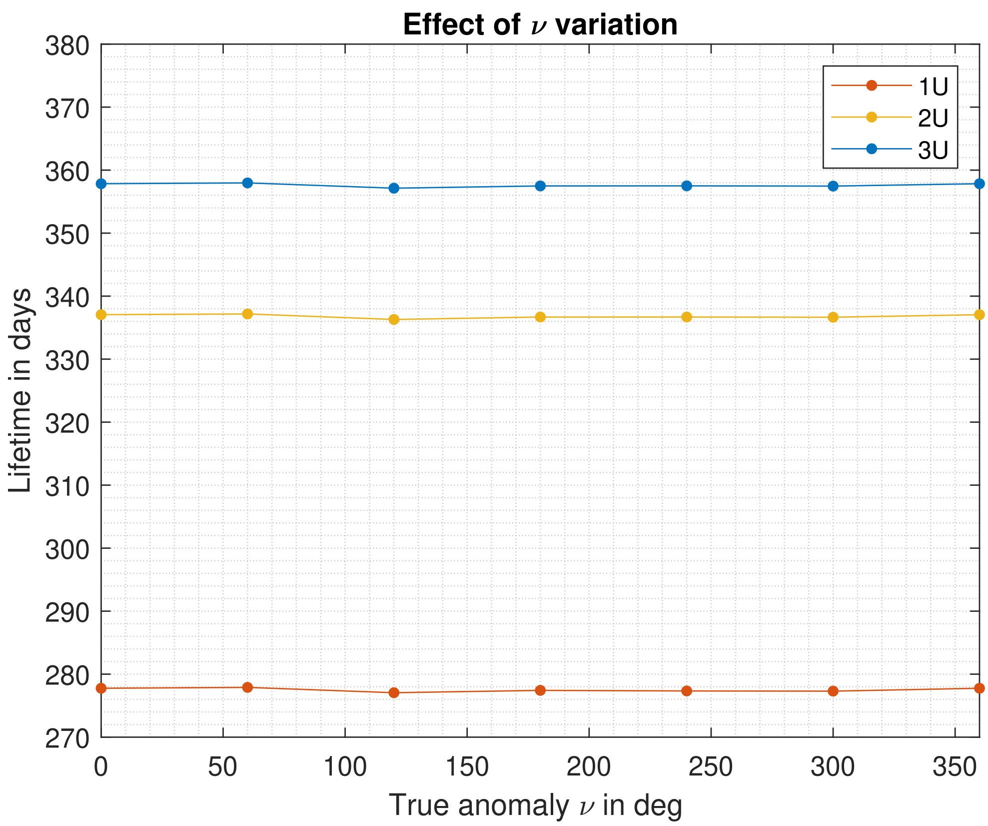

Figure 5.1: Satellite position in orbit study

The three-lifetime lines show the same nearly linear trend. The same applies if the Ω changes as shown in figure 5.2. Furthermore, this analysis provides a general assessment of the lifetime for CubeSat releasing from the ISS the 1^{st} October 2022. Considering the size of the CubeSat, approximately the decay time for a 1U is 277 days and 337 days for a 2U. Even longer is the decay time of a 3U, about one year (357 days exactly).

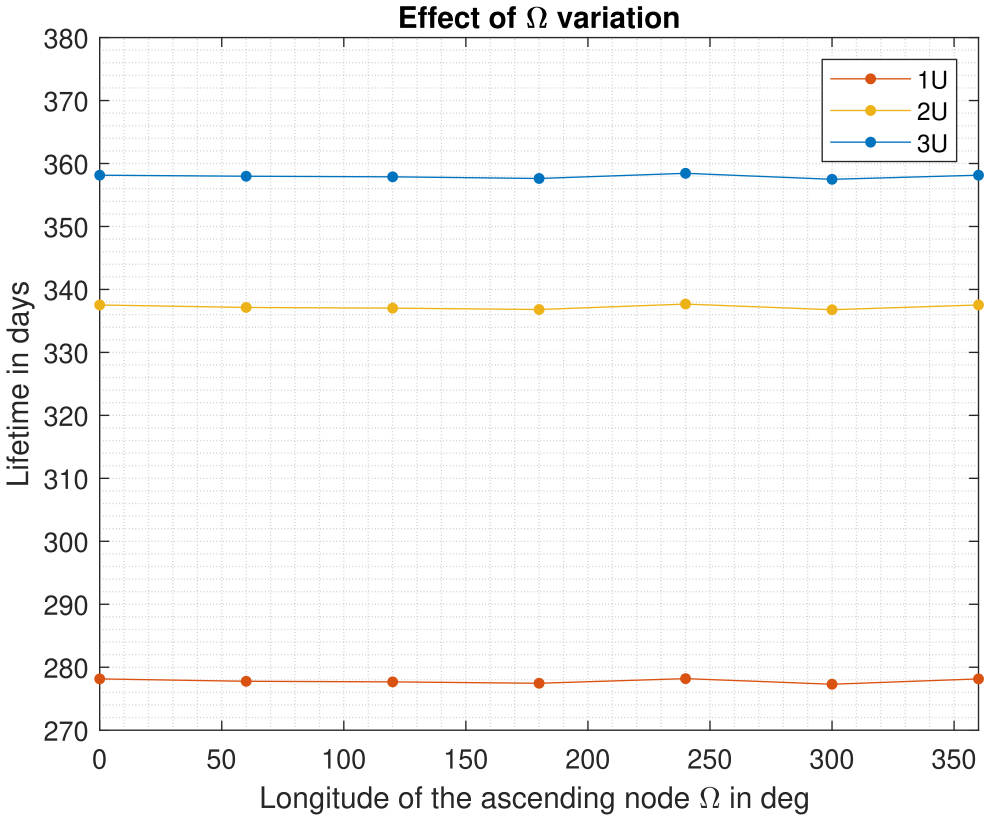

Figure 5.2: Ω study

Finally, these results show that by setting the deployment date and spacecraft parameters (C_D, XA and m), choose in the Astrogator's MCS the *Follow segment* with ISS as *Leader Vehicle* or the *Initial State segment* entering the ISS orbital elements as those of the CubeSats makes no difference.

5.2 Deployment altitude

According to the simulation, an increase in deployment altitude results in a longer lifetime, regardless of the size of the satellite and the type of atmospheric density model used. As expected, the higher the altitude, the lower the perturbative effect of the Earth's atmosphere, and the decay time rises.

Generally, there is no drastic difference in the performance of 2U and 3U. On the other hand, the estimated lifetime of 1U is always shorter than the others, and the difference increases as the deployment altitude changes. The reason for this pattern lies in the ballistic coefficient. In particular, in the motion equation appears the inverse of β. Trascurating the C_D, the area-mass ratio of 1U is the biggest and equal to 0.0147 $\frac{m^2}{kg}$. Therefore, the perturbative effect due to atmospheric drag is strongest on the 1U and its lifetime is the shortest one.

Figures 5.3, 5.4, 5.5 provide further details on the lifetime trend as deployment altitude and atmospheric density model vary.

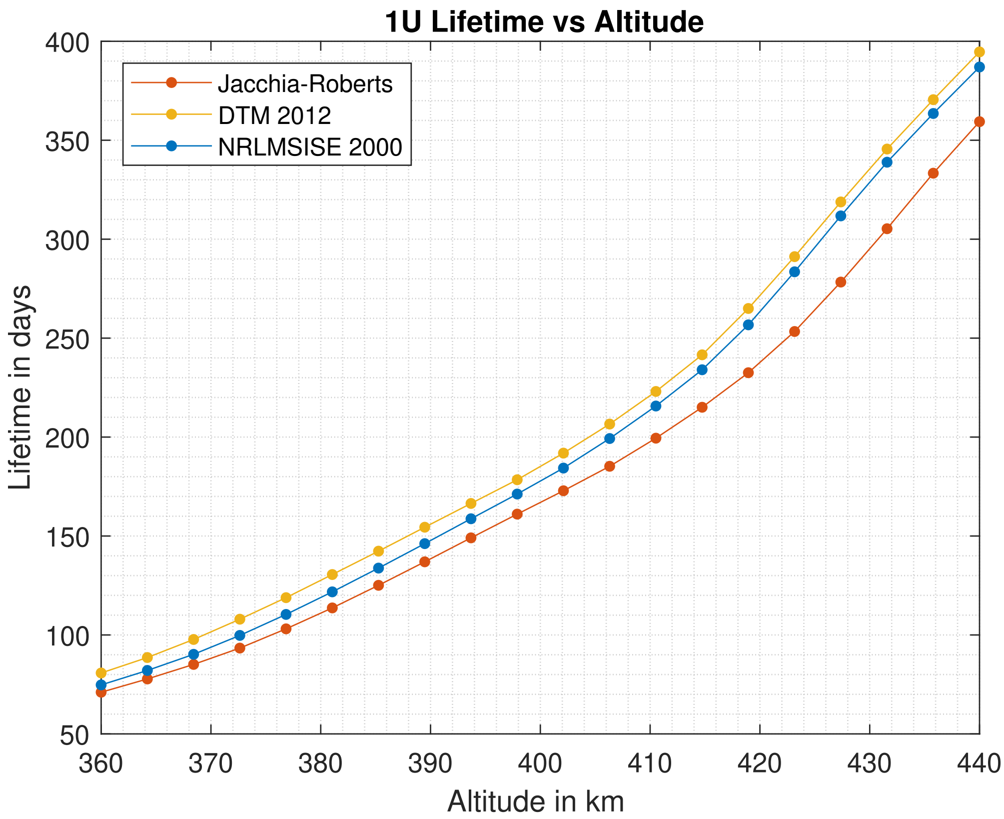

Figure 5.3: Effect of varying deployment altitude on 1U lifetime

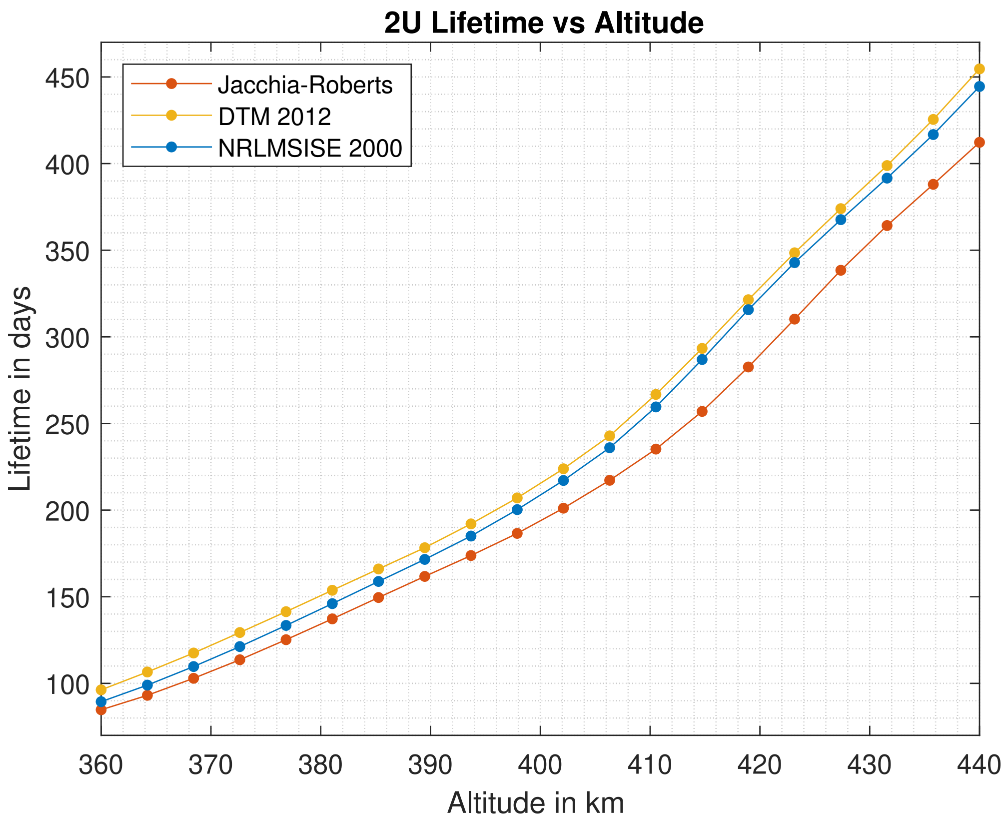

Figure 5.4: Effect of varying deployment altitude on 2U lifetime

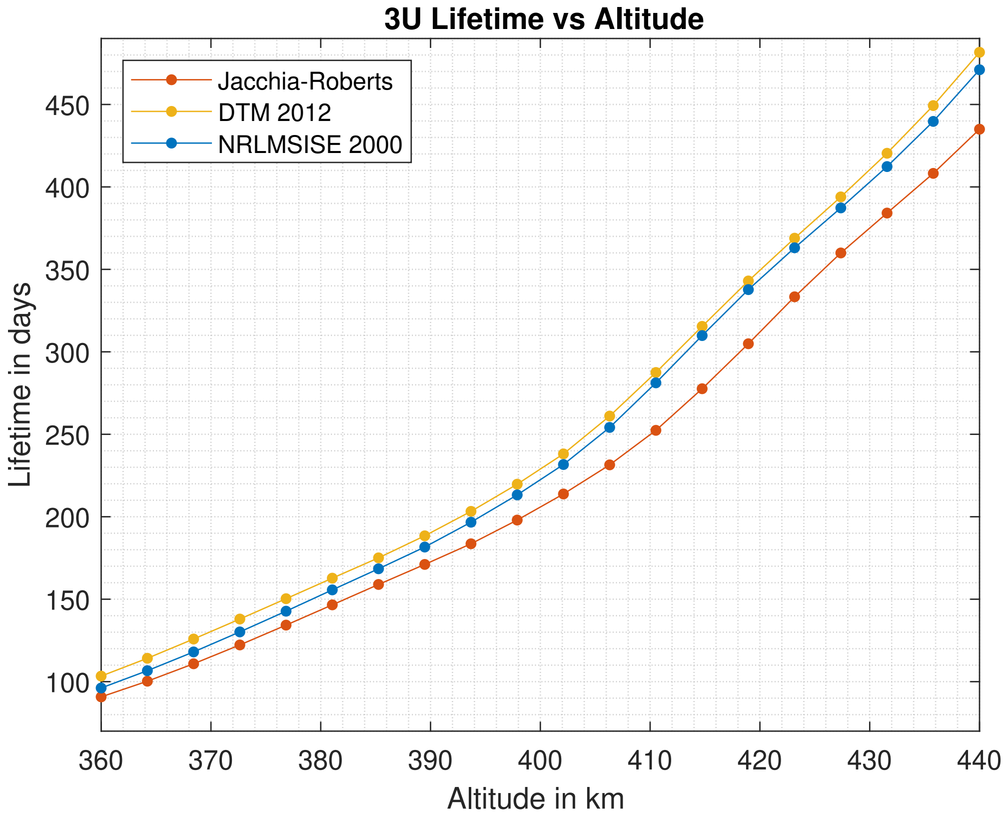

Figure 5.5: Effect of varying deployment altitude on 3U lifetime

Under 360 km, the lifetime is less than 100 days in all cases, whereas from 400 km to 440 km the CubeSats could remain in orbit for 200 days to 1.3 years. As shown in figure 4.5, in recent years the altitude of the ISS has fluctuated between 410 km and 420 km so this range may be more interesting. Specifically, at 415 km (i.e. equal to 6792 km considering the Earth radius of 6378 km), the decay time of the 3U is 310 days, while that of the 2U is 287 days. Even shorter is the decay time of 1U, 234 days.

For all CubeSat types, considering *NRLMSISE 2000* or *DTM 2012* as atmospheric density model implies similar lifetime evaluations, while *Jacchia-Roberts* provides always a shorter lifetime. This gap rises with altitude. Considering a 3U, STK allows the value of density over time to be evaluated accounting for the type of atmospheric density model chosen. Therefore, figure 5.6 shows the variation of density over time according to the chosen density model, while figure 5.7 shows how the altitude of the CubeSat goes down with time according to the density model. Specifically, the graph in figure 5.6 plots density values using a logarithmic scale in base 10, due to the enormous difference between values at high altitude (on the order of 10^{-3} kg/m^3) and those at low altitude (from 10^{-1} to 22 kg/m^3 at 120 km). Note that already at high altitudes, the three density models have different values. Although the latter are not significantly different from each other, there is a faster decay for 3U, whose lifetime is evaluated with *Jacchia-Roberts*. The trends of *DTM 2012* and *NRLMSISE 200* are similar up to an altitude of about 320 km. Below this altitude, the latter predicts higher density values and so the final lifetime is shorter than that evaluated with the former of 6 days. Approximately below 200 km, the density values are similar among both density models and increase rapidly as altitude reduces.

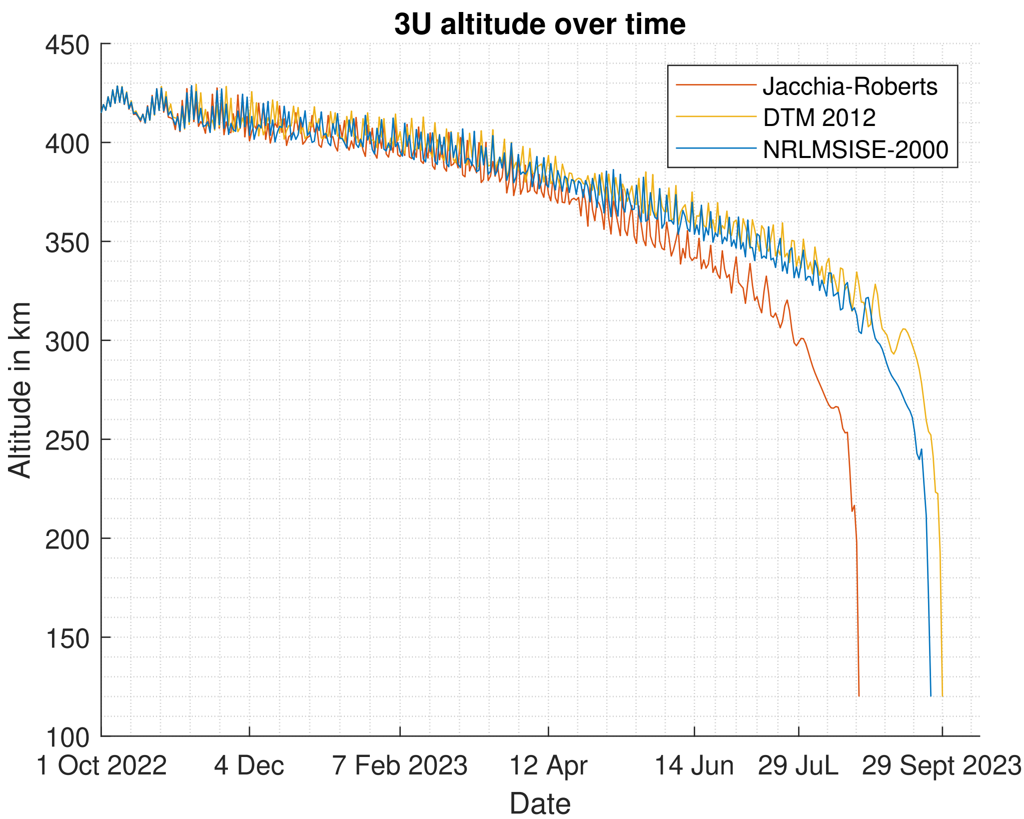

Figure 5.6: Lifetime of 3U depending on the density model chosen

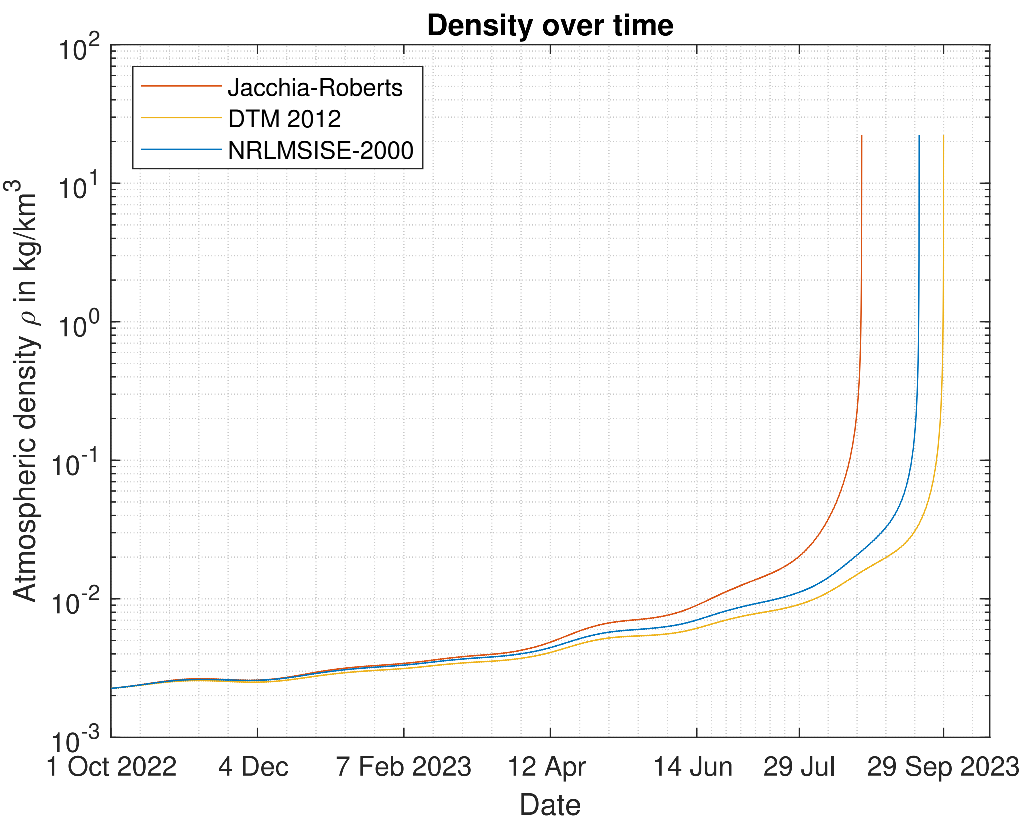

Figure 5.7: Comparison density model

Both *Jacchiara-Roberts*, *DTM 2012* and *NRLMSISE 2000* contain geomagnetic and solar flux indices and are therefore suitable for a valid lifetime estimate. The differences in the prediction of orbital decay lie in the number of atmospheric drag data incorporated as the basis of their basic assumptions, which in the latter two methods are greater than in the former because they are more recent [5]. Nevertheless, considering a possible error of one month in the lifetime prediction, *Jacchia-Roberts* can be chosen to reduce the calculation time. In fact, as shown in 5.1, it works very fast, especially if 1 s and 60 s are entered in the integrator settings as the minimum and initial steps respectively. These values are the defaults for RKF 7(8), but in this work, 300 s and 350 s are included in the integrator settings as initial and minimum steps respectively. It is evident from the table 5.1 that this choice results in a 6-day difference in the prediction of orbital decay, but enables a drastic reduction in computational time.

Table 5.1: Computational time analysis

Density model	Jacchia-Roberts	DTM 2012	NRLMSISE 2000
Initial step = 60 s, Min step = 1 s, Max step = 86400 s			
Time	96 s	120 s	148 s
Decay date	18 Aug 2023	24 Sep 2023	18 Sep 2023
Initial step = 300 s, Min step = 300 s, Max step = 86400 s			
Time	19 s	24 s	29 s
Decay date	24 Aug 2023	29 Sep 2023	23 Sep 2023

5.3 Deployment date

Figure 5.8 compares the two solar flux files downloaded from STK. It should be noted that the values are forecasts, except for the data of *SpaceWeather.txt* until 31^{th} December 2021, which are observed data. Moreover, in *SpaceWeather.txt*, up to 13^{th} February 2022, there are daily data, whereas after that date only monthly data related to the first day of the month. In contrast, *SolarFluxCSSI.dat* contains only monthly data. The values plotted in figure 5.8 are daily, so those up to 13^{th} February 2022 for *SpaceWeather.txt* are average values. As observed, *SolarFluxCSSI.dat* and *SpaceWeather.txt* have a similar mountainous trend until 2030. Thereafter, the former repeats its trend with higher peaks, while the latter shows anomalous behaviour predicting a minimum solar activity of about 10 years. The *SolarFluxCSSI.dat* essentially duplicates the data of the current solar cycle and scales it slightly according to what is expected to happen. On the other hand, the strange trend of *SpaceWeather.txt* is due to the high uncertainty in predicting $F_{10.7}$ values for the next solar cycle. For this reason, a date range from 2022 to 2030 is chosen in the *Deployment date analysis*. This temporal range is not suitable for predicting a lifetime of more than eight years, but this is not the case for the CubeSats chosen in this thesis.

As expected, the solar flux files pattern affects the estimated decay time. Particularly, lower values of $F_{10.7}$ correspond to a longer time in orbit for CubeSats, while higher values of $F_{10.7}$ correspond to faster decay. The reason lies in the influence of solar activity on the Earth's atmospheric density and, consequently, on the atmospheric drag and satellite decays.

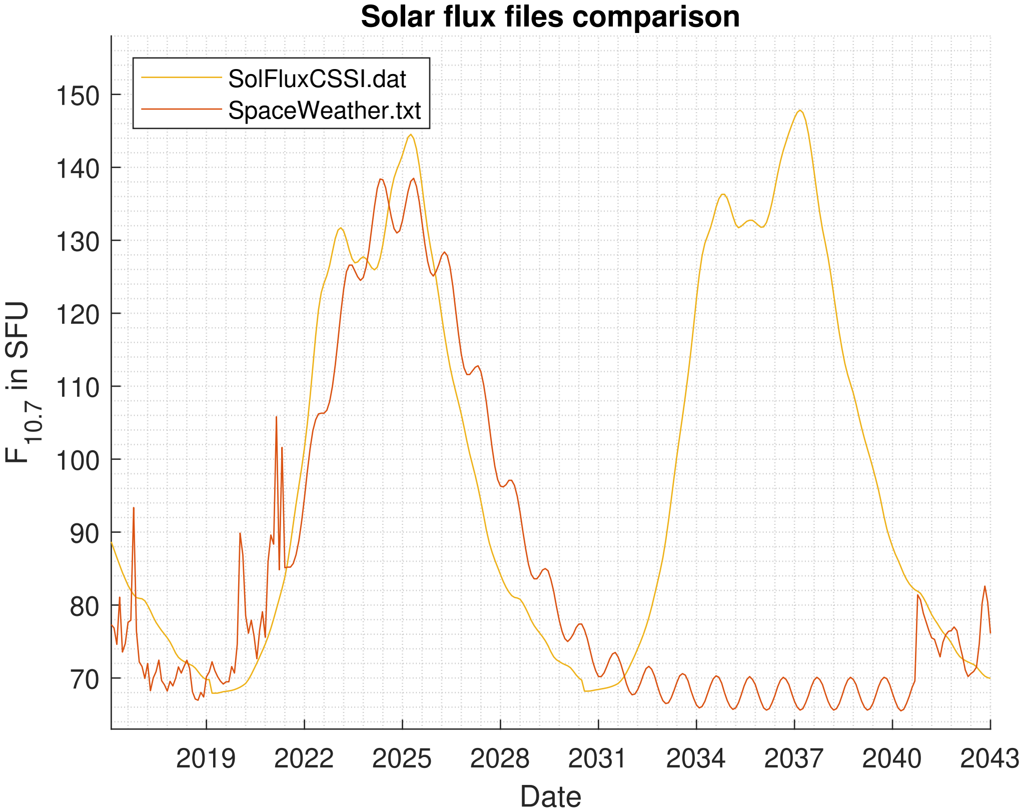

Figure 5.8: $F_{10.7}$ values over the years

Figures 5.9, 5.10, 5.11 show more details on the effect of deployment date on CubeSat lifetime as the solar flux file changes. In the period of the analysis, the two solar flux files show an alternating pattern for a specific period in which one predicts higher $F_{10.7}$ values than the other and vice versa in the subsequent period. In all three analysed cases (1U, 2U, 3U), in fact, the lifetime evaluated by considering *SpaceWeather.txt* as the solar flux file is longer than the other case from 2022 to 2025 while it is shorter from 2025 to 2030. The choice of one or the other flux file implies a difference in decay time from days to about three months, regardless of satellite size. The maximum difference occurs deploying in 2028, while the minimum is in 2024.

It is interesting to note what occurs during the maximum solar activity, which in this twenty-fifth cycle is expected for 2025. Considering *SpaceWeather.txt*, it is expected to decay in 198 days for 3U, whereas in 186 days for 2U. Even faster for 1U, 157 days. The difference between these values lies in the ballistic coefficient, which for the 1U is the lowest. Moreover, the lifetime reduction during this period is very drastic when compared to the value estimated in section 5.1. On the other hand, the decay is slower during the minimum solar activity that could occur from 2028 onwards. In particular, considering *SpaceWeather.txt* and deploying in 2030, the lifetime is 1.5, 1.9 and 2.1 years for 1U, 2U and 3U respectively.

Eventually, considering *SpaceWeather.txt*, the average lifetime is 290, 360 and 390 days for 1U, 2U and 3U respectively. Instead, considering *SolarFluxCSSI.dat*, the lifetime is about 30 days longer for each category. The performances of 2U and 3U are similar because of the similar β, which is not very different between them.

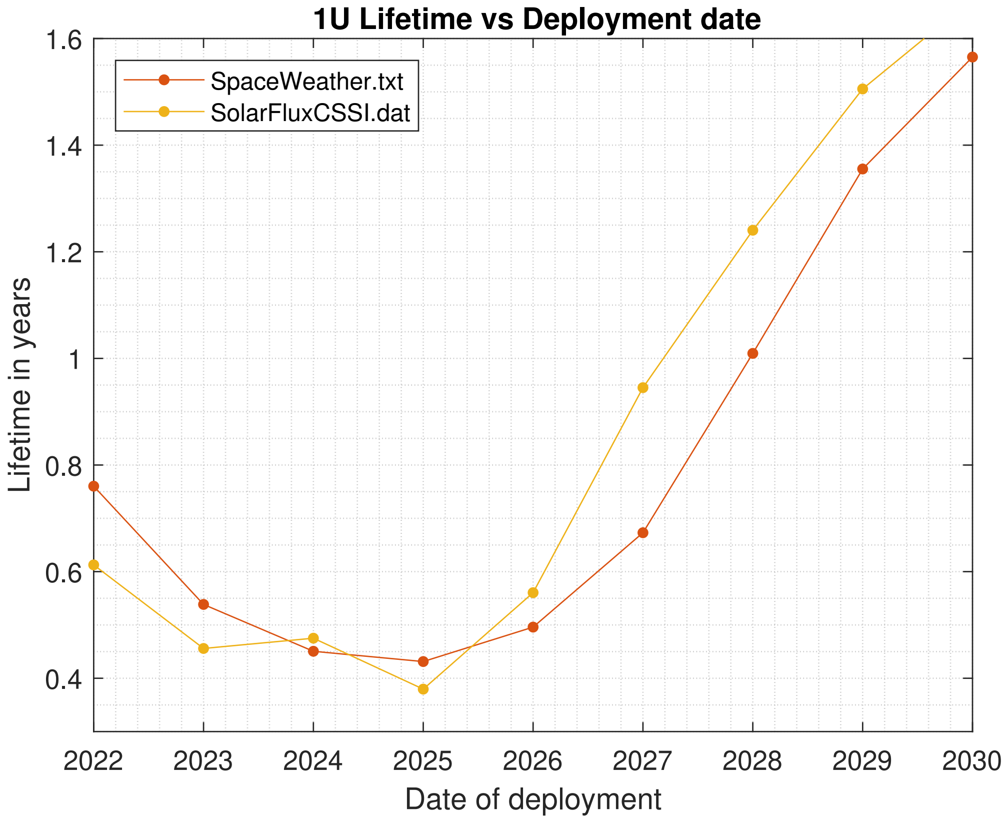

Figure 5.9: Effect of varying deployment date on 2U lifetime

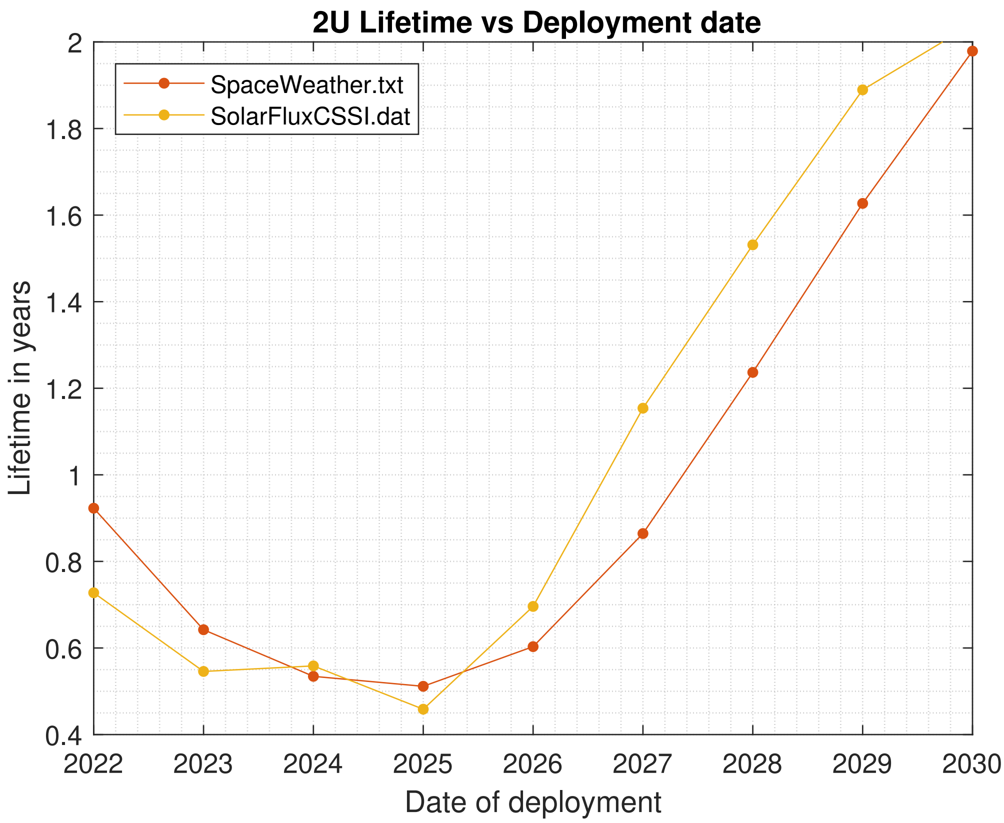

Figure 5.10: Effect of varying deployment date on 3U lifetime

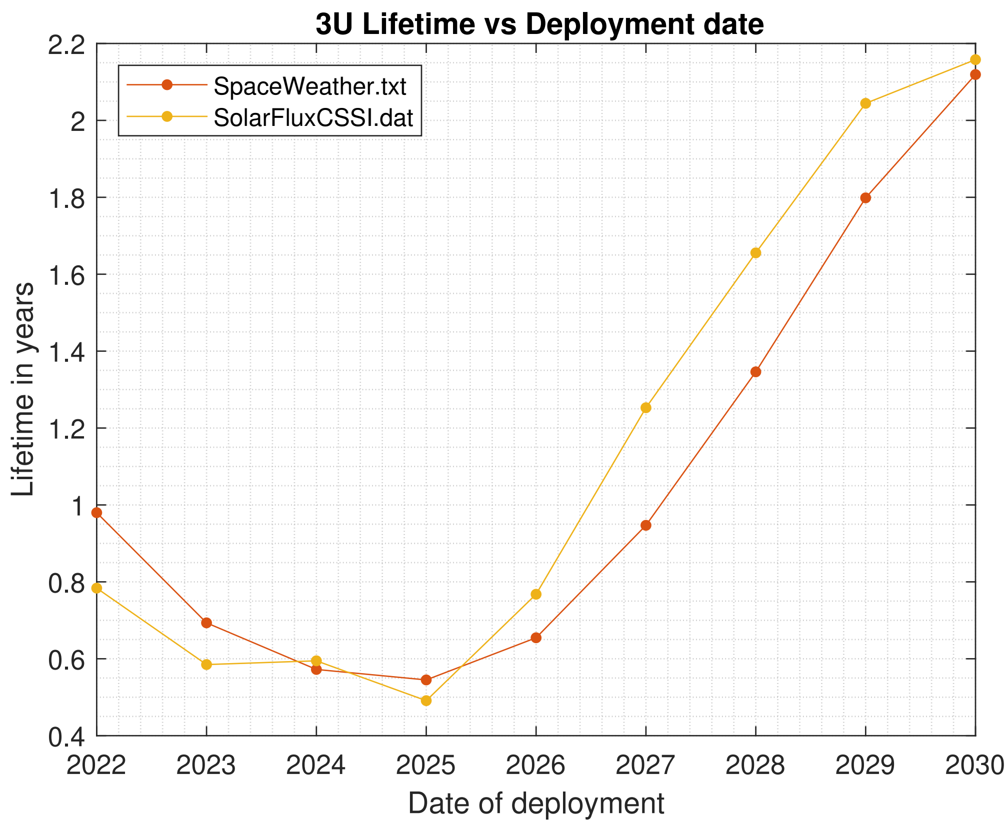

Figure 5.11: Effect of varying deployment date on 1U lifetime

5.4 Parametric study

Figures 5.12, 5.13 and 5.14 show the result of the third simulation. The blue line represents the lifetime trend, while the red line is the ballistic coefficient. As described in section 2, the drag perturbation is inversely proportional to β. As a consequence, the red line also describes how the variation of the spacecraft parameters can affect the motion perturbation of satellites.

The CubeSat attitude is also taken into account in this simulation. The way to model a satellite attitude in this simulation is by varying their cross-sectional area. Three attitudes and consequently three different drag areas are identified:

Minimum drag To consider *Minimum drag* as satellite attitude the smallest drag area is selected.

Gravity gradient To consider *Gravity gradient* as satellite attitude the greatest surface of the CubeSat is selected.

Tumbling To consider *Tumbling* as satellite attitude the averaged drag area is selected.

Concerning the general tendency, the higher the C_D value, the shorter the evaluated CubeSat lifetime. Similar behaviour occurs as the cross-sectional area varies. Conversely, the greater the mass of CubeSat, the longer it remains in orbit. Even β and lifetime have the same trend: if β rises, the decay time lengthens, while if β goes down, the decay time shortens. Eventually, it is noticed that the ΔV has a negligible influence on the satellite's decay. Specifically, increasing the deployment ΔV reduces

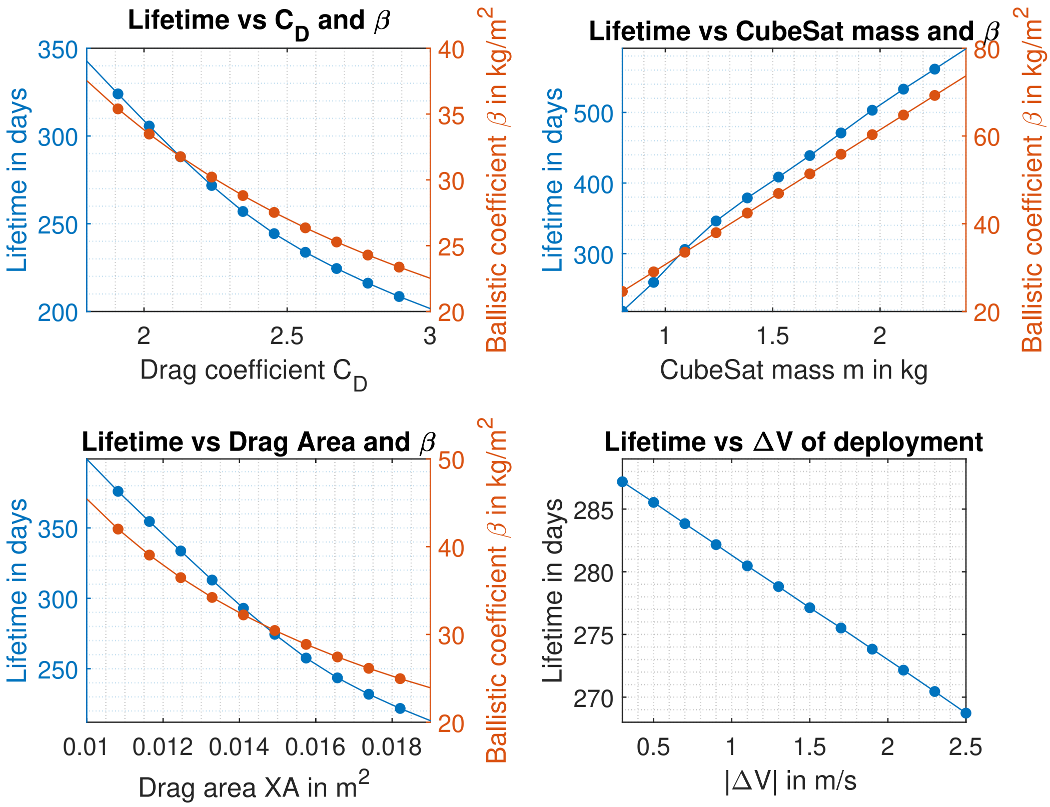

Figure 5.12: Parametric analysis for 1U

the lifetime by a few days. It should be noted that ΔV values depend on the satellite's physical properties and the limit imposed by deployers. As a consequence, a small impulse from the deployer may not be sufficient to avoid the satellite's return and collision with the deployer or with ISS. This parameter is regulated by [17].

Regarding 1U results (figure 5.12), a rise in C_D value from 2.2 to 3 reduces the lifetime by about 50 days. Specifically, it is noticed that as the β continues to go down, the reduction in lifetime is less and less. The same occurs in the XA case, with approximately the same reduction rate (maximum 23 days per step to minimum 7 days per step). However, a significant impact occurs with a greater satellite's mass: a mass of 2 kg entails a lifetime of about 1.4 years, whereas in the nominal case (m equal to 1 kg) it is only 277 days (just over half). In this case, the increase in β leads to a greater increase in decay time than its decrease in the C_D case and is roughly constant (about 30 days per step). It's relevant to observe that a massive CubeSat minimises the drag perturbation when other terms are considered fixed.

The trend of β is also similar in the 2U and 3U cases. However, there is a different time interval between decay evaluations as the XA changes. Considering 2U, the reduction is 100 days at the first variation of XA, while it becomes 19 days at the last. Even longer is the case of 3U, which goes from 200 days to 23 days.

It is observed that a 2U weighing 3 kg, has a lifetime of 1.25 years. In contrast, a 3U with the same weight has a lifetime of 0.99 days. Obviously, the difference lies in the different drag areas and, consequently, in the different value of β.

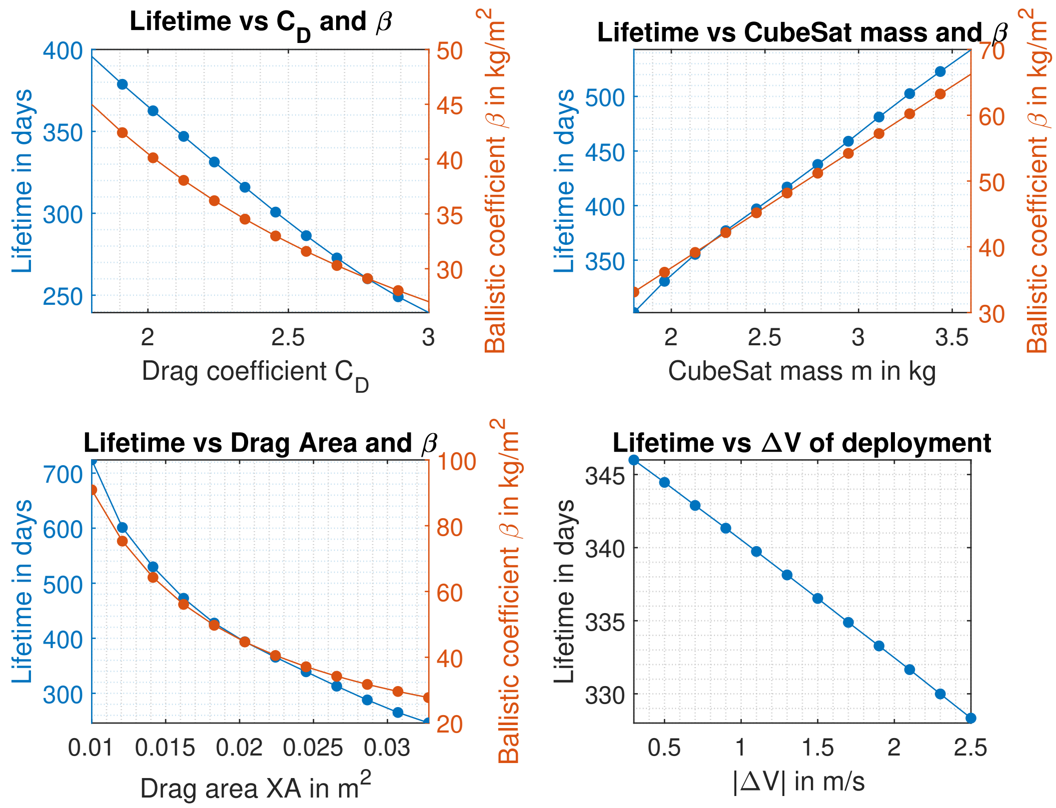

Figure 5.13: Parametric analysis for 2U

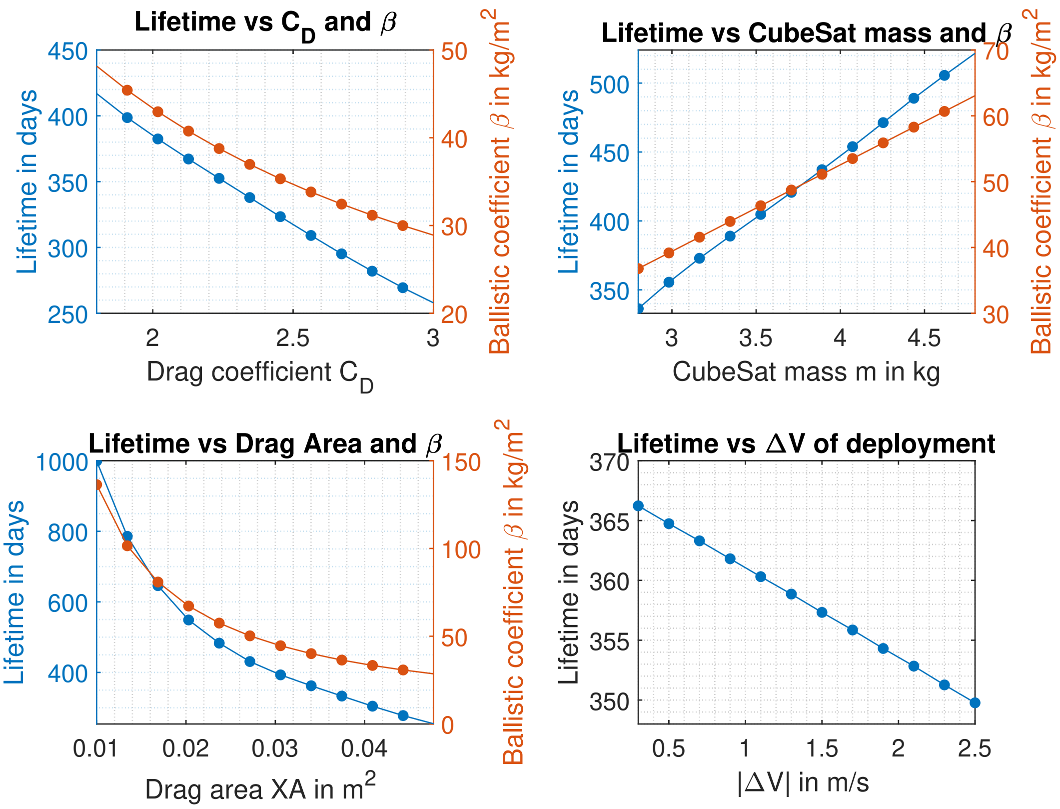

Figure 5.14: Parametric analysis for 3U

Table 5.2 shows the estimated lifetime of satellites as their attitude changes. Interestingly, the difference between the decay of 1U, 2U and 3U CubeSats in nominal mode (*Tumbling* attitude and nominal characteristics (table 4.1)) are in terms of months, whereas they are similar in the case of *Gravity gradient* attitude. On the other hand, it becomes huge in *Minimun drag* conditions. In fact, in the *Tumbling* case, the mass-area ratio (i.e. β disregarding the C_D which is considered 2.2 for all satellites) is equal to 100 $\frac{kg}{m^2}$ for all CubeSats, while in *Minimun drag* mode, β value for 1U, 2U and 3U is 100, 200 and 300 $\frac{kg}{m^2}$ respectively.

Table 5.2: Attitude analysis

Satellite	**Minimum drag**		**Gravity gradient**		**Tumbling**	
	XA	Lifetime	XA	Lifetime	XA	Lifetime
1U	100 cm^2	1.1 yr	100 cm^2	1.09 yr	148 cm^2	0.75
2U	100 cm^2	1.98 yr	200 cm^2	1.08 yr	247 cm^2	0.93
3U	100 cm^2	2.74 yr	300 cm^2	1.07 yr	346 cm^2	0.99

Another way to decrease the atmospheric perturbation is to reduce the cross-sectional area of the CubeSat, e.g. by modifying the geometry of the satellite during the design phase or by modifying its attitude along the orbit. An example of this effect on decay time is shown in figure 5.15.

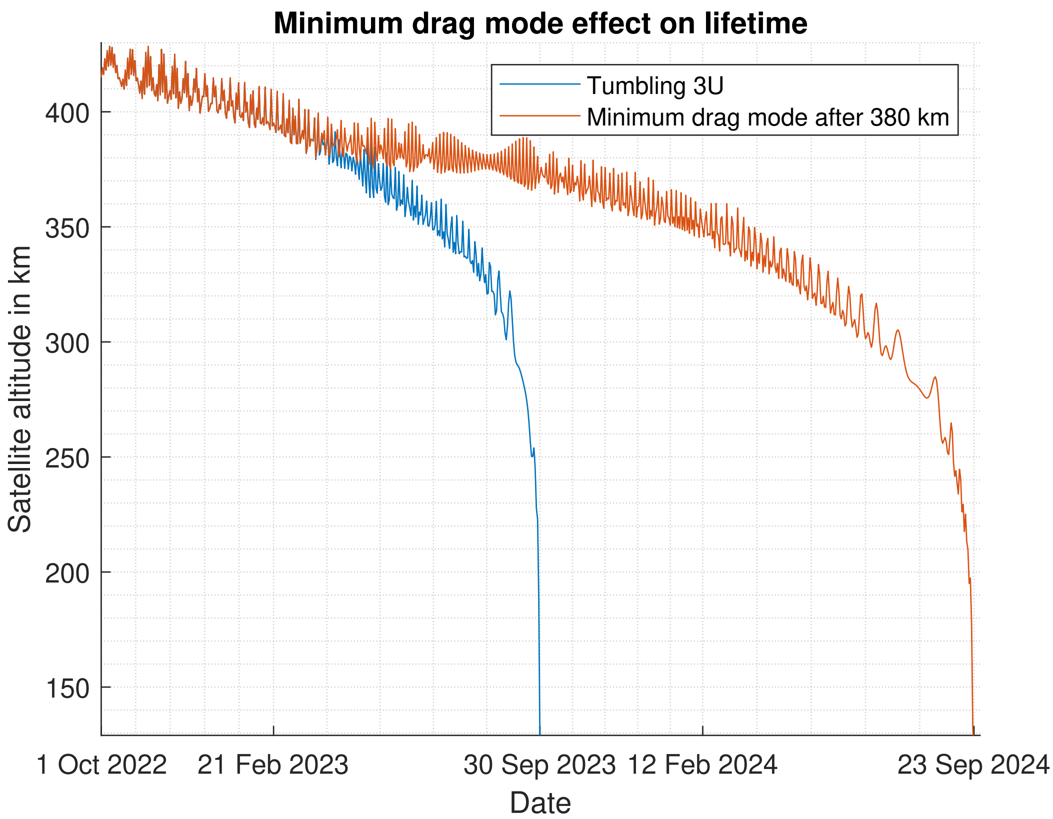

Figure 5.15: Effect of changing attitude on lifetime

In the condition of *Minimum drag* the 3U life is 2.74 years, about three times the value in the nominal case (table 5.2).

With a XA equal to 0.01 m^2, β is equal to 45.45 $\frac{kg}{m^2}$. This value of XA also corresponds to both the *Minimum drag* case and the *Gravity gradient* case. Actually, an extendable boom will be required to guarantee this second case. As highlighted in the table 5.2, with a XA of 0.01 m^2 the value of lifetime is 1.09 years while considering the averaged area of 0.0148 m^2 it is approximately 0.75 years.

The typical life of a default 2U with a tumbling attitude is approximately 357 days. If a longer time in orbit is desired, the cross-sectional area can be reduced. With a XA equal to 0.02 m^2, the satellite remains in orbit for 37 more days.

5.5 Drag sail

According to the *Drag sail* analysis, the sooner the drag sail unfolds, the faster the decay will be. As observed in section 5.4 and the area of the drag sail being the new XA of the satellite, a larger one implies a shorter time in orbit. Figure 5.16 show the pattern of the lifetime as the altitude of deployment of the drag sail and the size of the latter change.

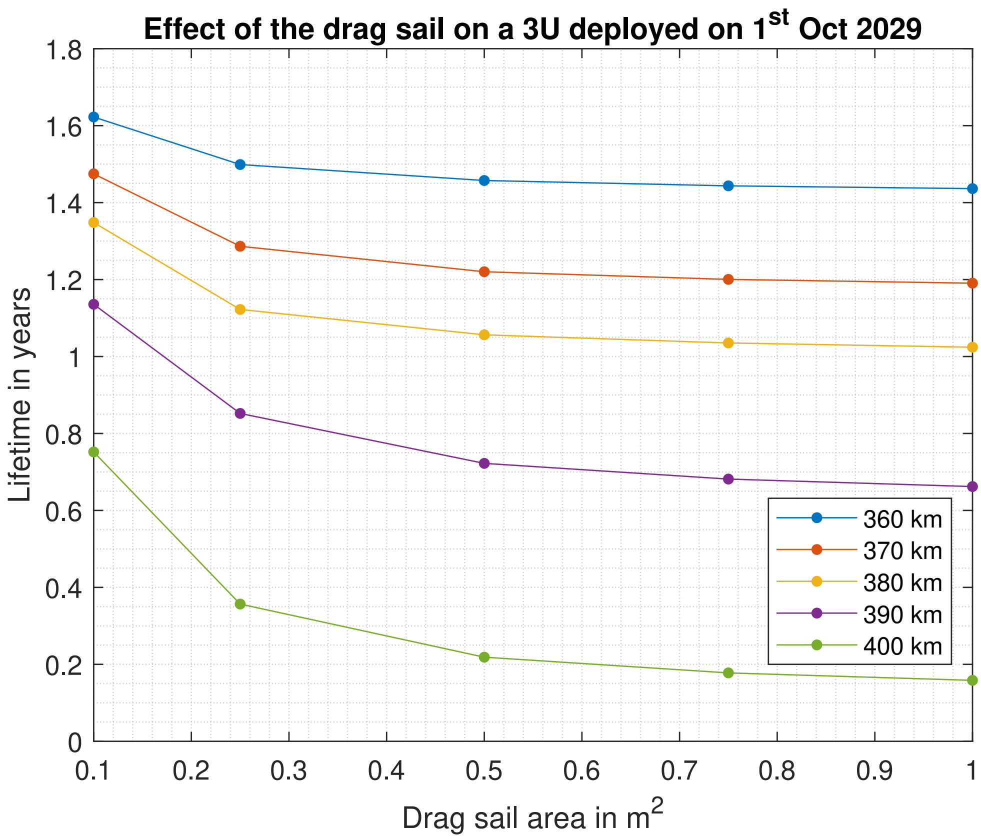

Figure 5.16: Effect of deploying a drag sail on lifetime

Deploying the drag sail at 400 km, it sufficient an area of 0.1 m^2 to reduce the 3U lifetime from roughly 600 days to 274 days. Using a device to increase the atmospheric drag is more efficient at high altitudes where the density is still low. Exploiting a drag sail of 1 m^2 when the CubeSat reaches 360 km entails a decrease of only 14% in the lifetime. A common trend is a small difference in decay choosing a drag sail of an area between 0.5 and 1 m^2. Contrastly, the rise in the area from 0.1 to 0.25 m^2 implies the biggest lifetime decrease.

Figure 5.17 shows an example of the effect of deploying a drag sail with an area of 0.25 m^2 on 3U orbital decay at 380 km. With this combination, it could be possible to have a life a month smaller than that of the 3U deployed in 2022 when the solar activity is more intense.

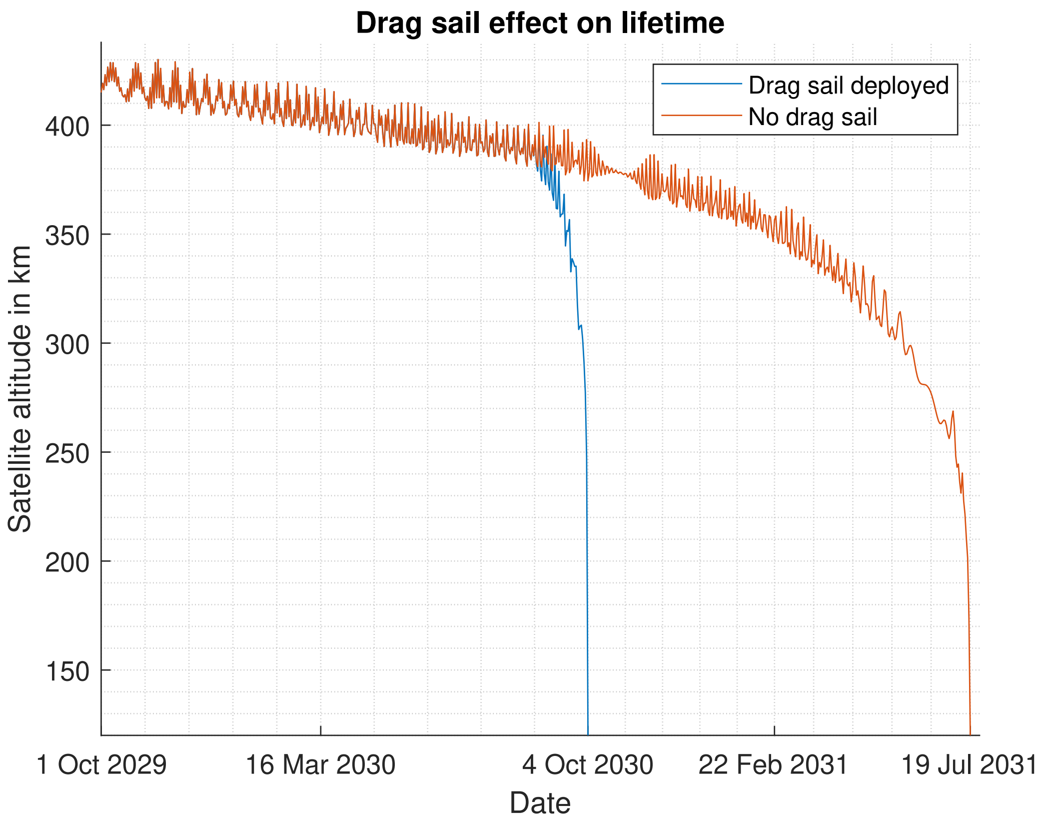

Figure 5.17: Effect of deploying a drag sail on lifetime

5.6 Deployment direction

In the last simulations, the effects of changing the direction of satellite deployment are studied. Figures 5.18 and 5.19 show the trend of the lifetime of 1U, 2U and 3U as the Az coordinate of the *Thrust Vector* changes, keeping El equal to 45° and 0° respectively.

In figure 5.18 is also plotted a vertical dashed black line representing the values of lifetime obtained in the nominal case (i.e. Az=180° and El=45°). Note that the three curves have a mirror-image pattern with respect to the nominal case. In fact, launching a CubeSat at 45° or 315°, at 135° or 225° and at 90° or 270° makes no difference in terms of the time a CubeSat stays in orbit. As a general trend, changing the deployment direction from the nominal one always means increasing the lifetime. On the one hand, deploying with Az equal to 135° and 225° leads to a negligible rise of the lifetime of about 1 or 2 days. On the other hand, deploying with Az equal to 0°, 45° and 315°, the lifetime goes up to 25 days longer for 1U and 22 for 2U and 3U.

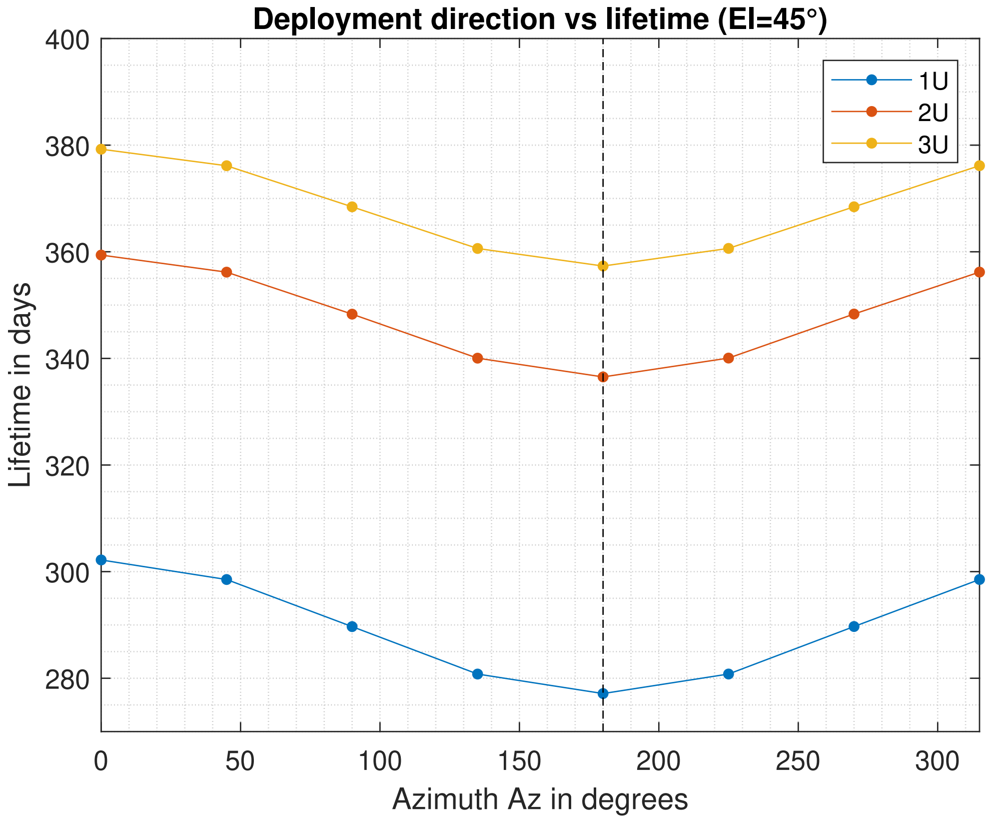

Figure 5.18: Effect of changing deployment direction keeping El equal to 45°

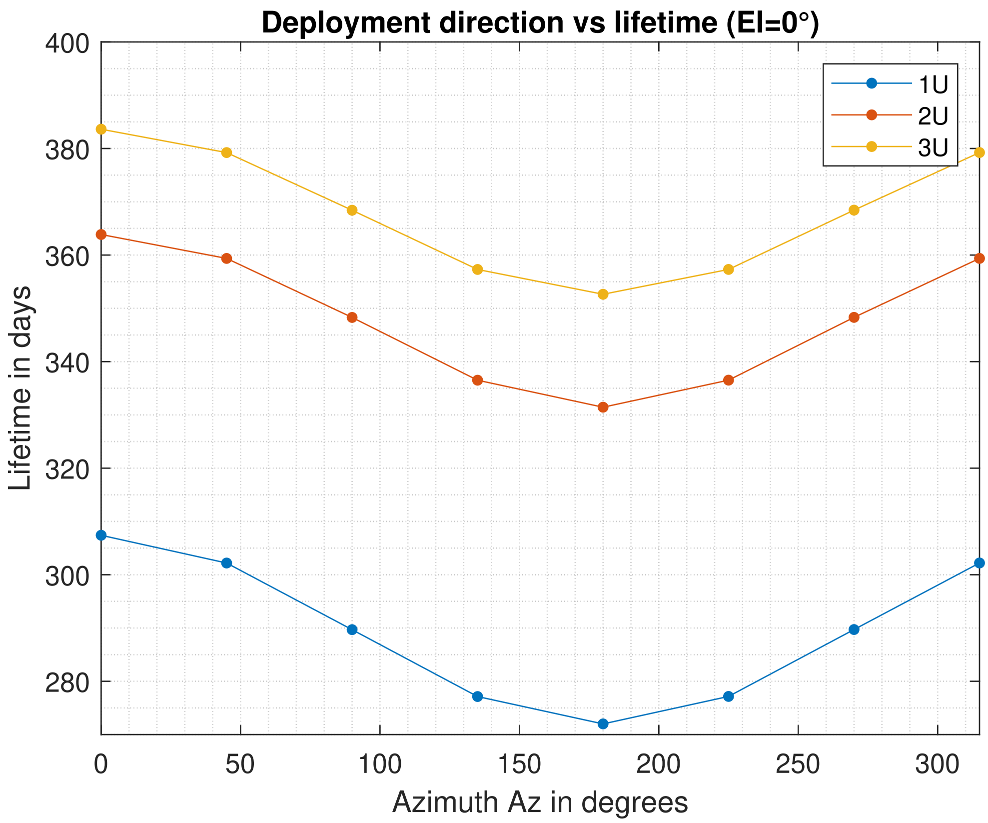

Figure 5.19: Effect of changing deployment direction keeping El equal to 0°

As is observed in figure 5.19, by choosing the El of the *Thrust Vector* equal to 0°, the three curves have a mirror-image trend with respect to the case where Az is equal to 180° but do not correspond to the nominal orbital decay (i.e. lifetime obtained when Az is equal to 180° and El equal to 45°) but to lower values. Instead, the nominal lifetime is obtained by launching the CubeSats at Az equals 135° and El equals 0°, Furthermore, in this second simulation the forward deployment implies longer lifetimes than in the previous simulation, while the backward deployment implies shorter lifetimes. The longest orbital decay is always obtained with 0° of Az and is longer than in the previous study, but only by about 5 days for each category of CubeSat. The reason for the increase in the duration of the time in orbit lies in the direction of the ΔV provided to the CubeSat: providing a forward impulse implies an increase in the semi-major axis of the orbit and consequently an increase in lifetime. This is true both for a thrust vector with El equal to 0° and equal 45° because in the latter case, there is also a component of ΔV in the direction of velocity.

Related to the deployment directions topic, the safety problem in terms of crush with the ISS is to be considered. Therefore, the range between CubeSat and ISS is plotted in figure 5.20.

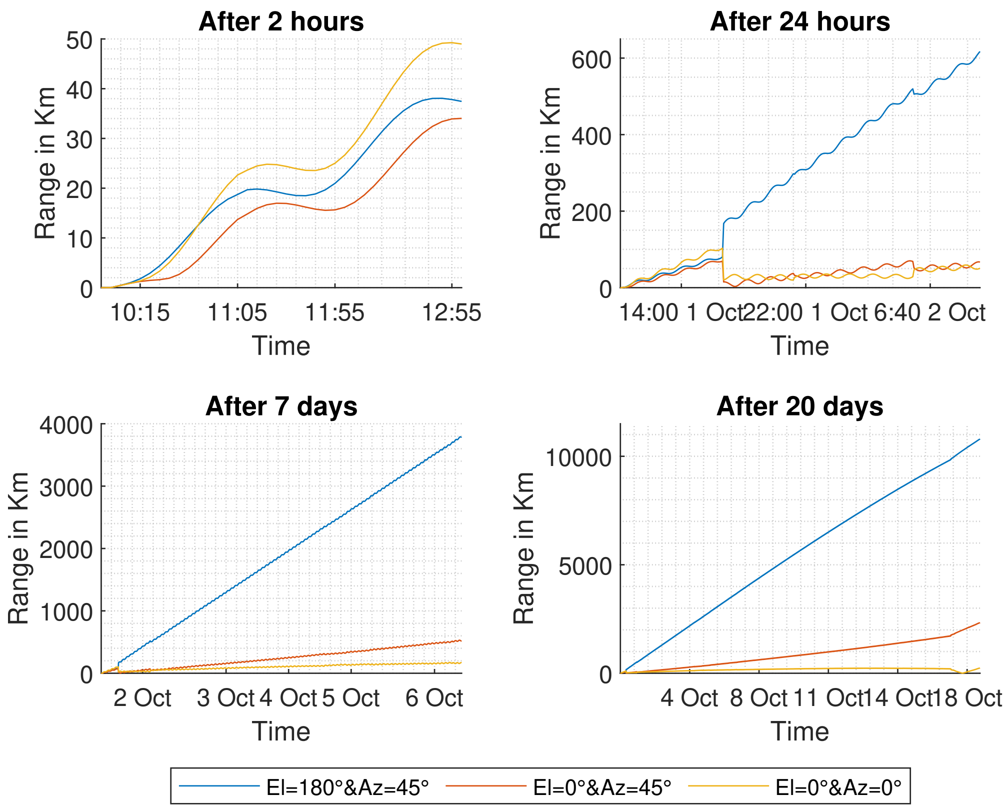

Figure 5.20: Range between ISS and CubeSat

In figure 5.20 are shown three of the cases studied: CubeSat deployment at Az equals 180° and El equals 45° (case 1), CubeSat deployment at Az equals 0° and El equals 45° (case 2) and CubeSat deployment at Az equals 0° and El equals 0° (case 3). The range between CubeSat and ISS over time is reported after 2 hours, 24 hours, 7 days and 20 days. Note that in case 1, the CubeSat after deployment continuously moves away, while the CubeSat in case 2 after moving away returns to a distance

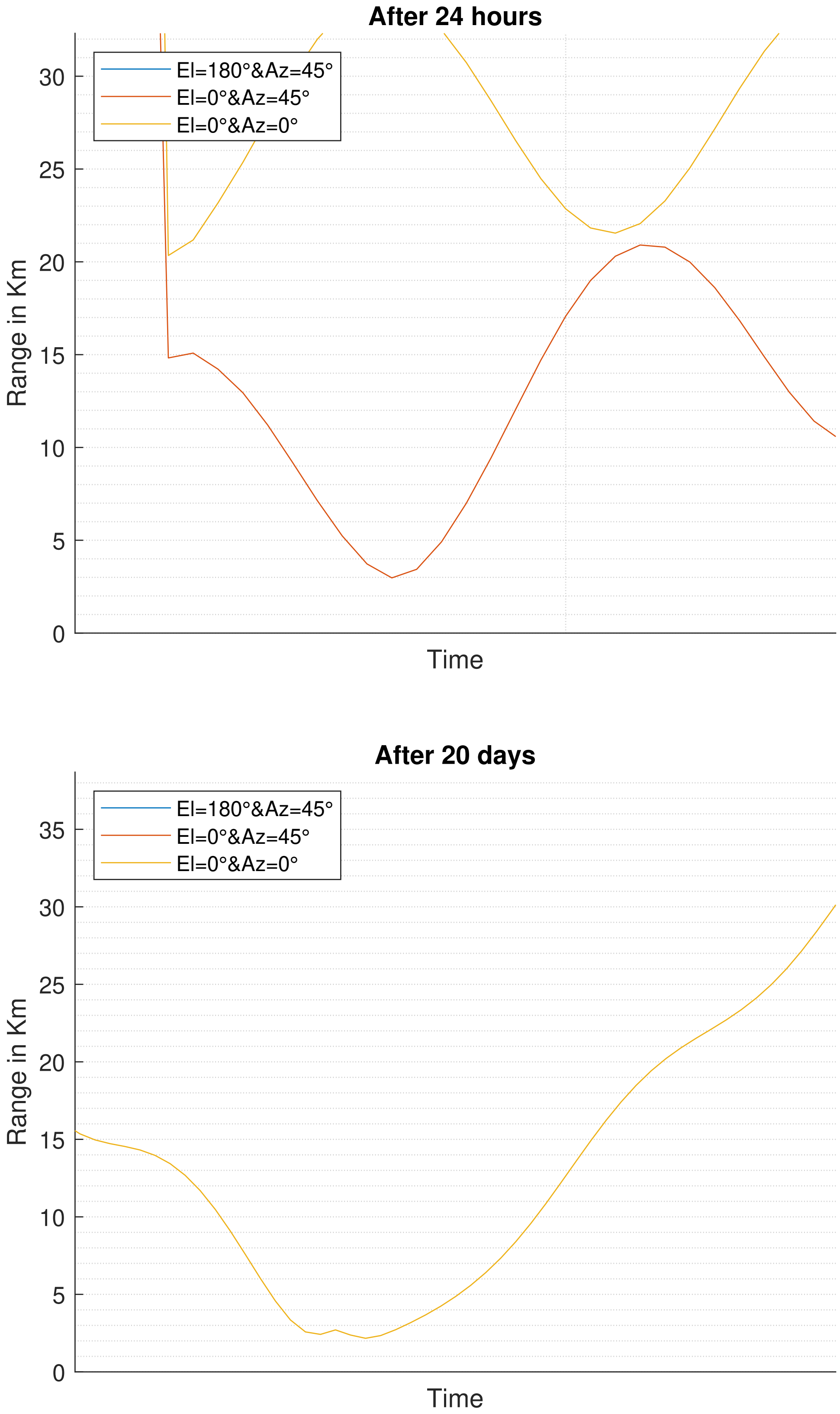

Figure 5.21: Range between ISS and CubeSat

of 3 km from the station on 1^{th} October at 17:00 and then moves away again. A similar trend occurs for the CubeSat in case 3, but it comes close to the station on 18^{th} October. Figure 5.21 shows an enlargement of cases 2 and 3 in figure 5.20 where both cases reach a distance from the ISS below 5 km. Therefore, a change of deployment direction shall be followed by a risk analysis to find out whether the minimum distances stated above are acceptable.

Chapter 6

Conclusion

This work has been performed through the various chapters where the specific topics have been developed. Chapter 1 describes the main features of the deployment of satellites from the ISS, and the study objectives and concludes with introducing the approach followed for the lifetime estimation. Chapter 2 describes the orbital dynamics useful to understand the orbital decay problem, and the perturbation techniques to propagate the orbit accounting for perturbations and concludes with an overview of the latter. Chapter 3 describes the main adopted STK capabilities, while chapter 4 reports about implementations of the different simulations and what the inputs are for each of them. Eventually, chapter 5 refers about the results of each analysis through tables, graphs and comments.

By using Astrogator as the STK propagator, the orbital decay of tumbling CubeSats with typical physical features has been investigated taking into account atmospheric drag, solar radiation pressure, moon and sun perturbations and the effect of the non-spherical Earth. In addition, solar activity has been also considered choosing density models that require geomagnetic and solar flux indices in input. Since foreseeing the time a satellite will remain in orbit is a difficult task with uncertain results, parametric analyses have been performed varying the possible parameters influencing the prediction to provide a predicted life span for different scenarios. Particularly, analyses of deployment altitude, date, directions and the ballistic coefficient have been carried out. According to this work:

- The lifetime of 1U, 2U and 3U CubeSats with a tumbling attitude and deployed from the ISS on the 1^{st} October 2022, is about 277, 337 and 357 days respectively.
- The reduction of the initial deployment altitude leads to a reduction in the duration of the time in orbit due to the high density at low altitudes. Therefore, an adequate atmospheric model, especially those that accommodate solar activity variations as described in the section 2.3.3 (high solar activity means high density fixing the altitude), plays a relevant role. However, the prediction of solar activity is still uncertain as shown in figure 5.8, thus the most recent atmospheric models shall be considered because they are based on more atmospheric drag data collected over the years [5].
- To foresee a lifetime longer than six years is necessary a *SolarFluxCSSI.dat* due to the uncertainty on the next solar cycle, otherwise, *SpaceWeather.txt* is usually recommended. Contrary to the nominal deployment date, the release of a CubeSat during solar maximum results in an orbital decay of 157, 186 and

198 days for respectively 1U, 2U and 3U. On the other hand, during the solar minimum, the lifetime is approximately doubled for all CubeSats.

- 2U and 3U CubeSats have similar trends in the different simulations due to their β being similar. In contrast, the ballistic coefficient of a 1U is lower than the former, for this, its lifetime is very frequently shorter.
- To counter atmospheric drag, the satellite's mass or reducing its XA shall be increased. The latter modification can also be made during its operational life by changing the satellite's attitude to *minimum drag mode* substantially increasing its lifetime. In particular, it has a greater influence on the lifetime of 2U and 3U, which rises from about 1 year to 2 and 3 years respectively.
- A drag sail of 0.25 m^2 could reduce the 3U's time in orbit during periods of intense solar activity to about one month less than the estimated duration during a normal period.
- Interestingly, deploying the CubeSat at 45° and forward increases the lifetime by about 25 days. The same effect is obtained if El is equal to 0°, but in both cases, safety analyses shall be carried out for the risk of collision between CubeSat and ISS.

To conclude the lifetime of a CubeSat deployed from the ISS could be affected primarily by the atmospheric drag and solar activity as environmental perturbation and by mass and cross-sectional area as physical properties. Nevertheless, the uncertainty of solar activity and the difficulty in the satellite's attitude prediction could be antagonists in accurate prevision. On the other hand, solar radiation pressure, CubeSat position in orbit, the majority of downward deployment direction and $|\Delta V|$ of deployment have little or no influence on CubeSats deployed at an altitude between 360 and 440 km.

Most of the numerous unknowns have been analyzed in this study and, several aspects of the lifetime of the CubeSat deployed from the ISS have been clarified. To obtain more precise results, this work could be further developed with more input data. An ad-hoc analysis of the satellite's attitude and C_D could be carried out. Other forms of CubeSat could be studied and a Monte Carlo analysis could improve the road map outlined in this work. Furthermore, by varying other STK settings, such as modifying the integrator adopted by HPOP and searching for pitch values that represent the right meeting point between fast computation times and precise results, customised solutions could be obtained according to the type of precision required.

Bibliography

[1] C. Cappelletti, S. Battistini, and B. Malphrus. *CubeSat Handbook: From Mission Design to Operations*. Elsevier Science, 2020. ISBN: 9780128178850. URL: `https://books.google.it/books?id=RTbDDwAAQBAJ` (cit. on pp. 1–3).

[2] Bruce Yost et Sasha Weston. «State of the Art of Small Spacecraft Technology». In: 2023 (cit. on pp. 1, 2).

[3] *NanoRacks CubeSat Deployer (NRCSD) Interface Definition Document (IDD)*. Nanoracks. 2018. URL: `https://nanoracks.com/wp-content/uploads/Nanoracks-CubeSat-Deployer-NRCSD-IDD.pdf` (cit. on pp. 3, 4, 36).

[4] Giuseppe Roccasalva. «CubeSats deployed from the ISS: development of a code to predict the orbital decay». In: 2023 (cit. on p. 4).

[5] Daniel Oltrogge and C.-C Chao. «Standardized approaches for estimating orbit lifetime after end-of-life». In: *Advances in the Astronautical Sciences* 129 (Jan. 2008), pp. 187–206 (cit. on pp. 4, 5, 37, 46, 59).

[6] Ai-Ai Lumnay C Cojuangco. «Orbital Lifetime Analyses of Pico- and Nano-Satellites». In: 2007 (cit. on p. 5).

[7] Cagri Kilic. «Deployment Effects Analyses for CubeSat Systems». PhD thesis. Jan. 2013 (cit. on p. 5).

[8] R.R. Bate, D.D. Mueller, J.E. White, and W.W. Saylor. *Fundamentals of Astrodynamics*. Dover Books on Physics. Dover Publications, 2020. ISBN: 9780486497044 (cit. on pp. 6–9, 11–14).

[9] David A. Vallado. «Fundamentals of Astrodynamics and Applications». In: 1997 (cit. on pp. 8–12, 14, 16–20).

[10] J.P. Vinti and G.J. Der. *Orbital and Celestial Mechanics*. Progress in astronautics and aeronautics. American Institute of Aeronautics & Astronautics, 1998. ISBN: 9781600864292. URL: `https://books.google.it/books?id=-dXzdYHvPgMC` (cit. on p. 15).

[11] R.M.L. Baker, M.W. Makemson, and M. Makemson. *An Introduction to Astrodynamics*. Academic Press, 1967. ISBN: 9780120756728. URL: `https://books.google.it/books?id=NKRTAAAAMAAJ` (cit. on p. 15).

[12] James R. Wertz, David F. Everett, and Jeffery J. Puschell. «Space mission engineering: the new SMAD». In: 2011 (cit. on pp. 15–17).

[13] A.C. Long, R. Pajerski, R. Luczak, United States. National Aeronautics, Space Administration, and Goddard Space Flight Center. *Goddard Trajectory Determination System (GTDS): Mathematical Theory*. Goddard Space Flight Center, 1989. URL: `https://books.google.it/books?id=X%5C_WdtgAACAAJ` (cit. on p. 20).

[14] J. L. Nayler. «Introduction to Orbital Mechanics. Franz T. Geyling and H. Robert Westerman. Addison-Wesley. 350 pp. Illustrated». In: *The Aeronautical Journal* 75.731 (1971), pp. 796–796. DOI: `10.1017/S0001924000046819` (cit. on p. 20).

[15] «https://help.agi.com». In: (cit. on pp. 21, 29).

[16] «http://celestrak.org/SpaceData/». In: (cit. on p. 24).

[17] «ISS Safety Requirements Document». In: vol. SSP 51721 baseline. Sept. 2019 (cit. on pp. 36, 50).